









Endothelial-to-mesenchymal transition in the fetoplacental macrovasculature and microvasculature in pregnancies complicated by gestational diabetes

Abigail R. Byford¹ , Georgia Fakonti¹ , Ziyu Shao¹, Sharanam Soni¹ , Sophie L. Earle¹ , Muath Bajarwan¹, Lara C. Morley¹ , Beth Holder² , Eleanor M. Scott³  and Karen Forbes¹ 

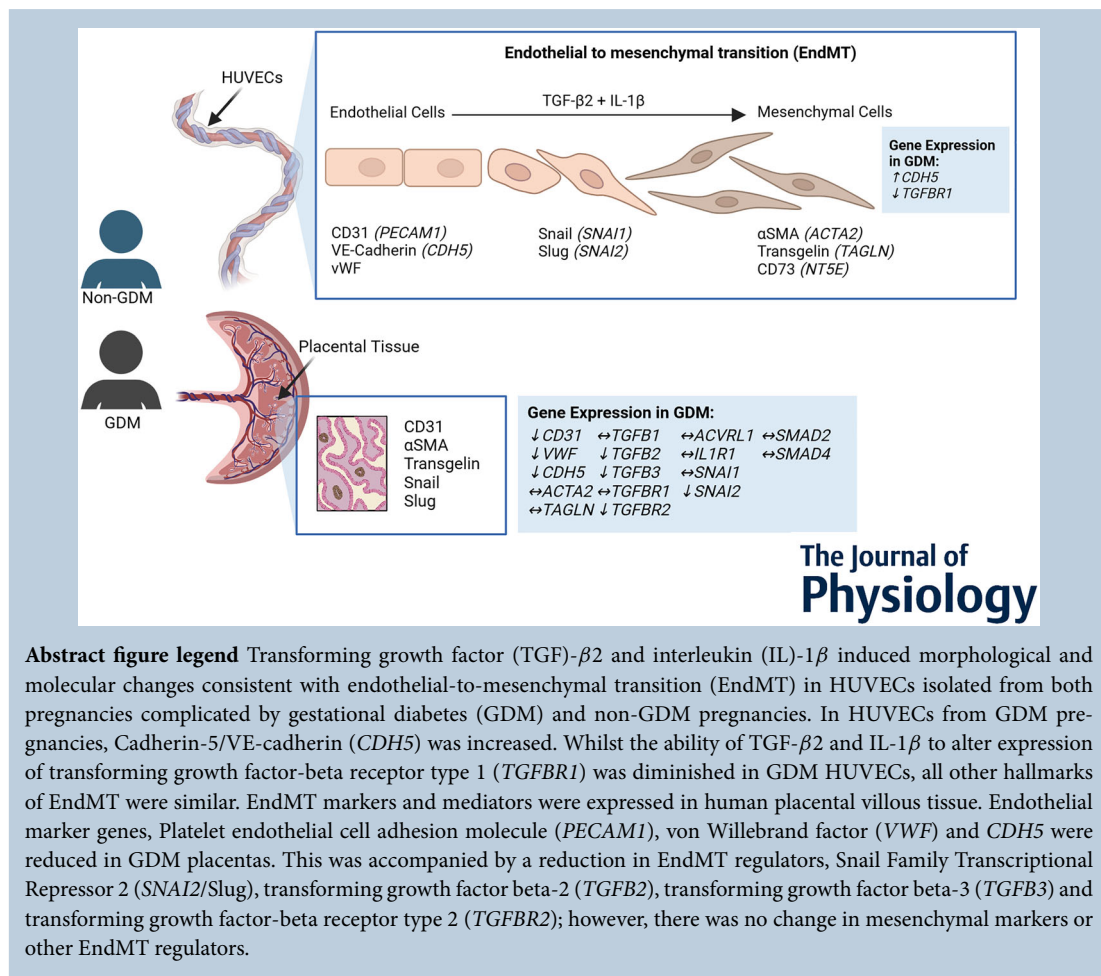
¹Discovery and Translational Science Department, Leeds Institute of Cardiovascular and Metabolic Medicine, Faculty of Medicine and Health, University of Leeds, Leeds, UK

²Institute of Reproductive and Developmental Biology (IRDB), Imperial College London, London, UK

³Clinical and Population Sciences, Leeds Institute of Cardiovascular and Metabolic Medicine, Faculty of Medicine and Health, University of Leeds, Leeds, UK

Handling Editors: Kim Barrett & Luis Sobrevia

The peer review history is available in the Supporting Information section of this article (<https://doi.org/10.1113/JP287931#support-information-section>).



A. R. Byford and G. Fakonti, contributed equally to this work.

Abstract Gestational diabetes mellitus (GDM) is linked to altered fetal development and an increased risk of offspring developing cardiometabolic diseases in adulthood. The mechanisms responsible are unclear; however, GDM is associated with altered fetoplacental vascularisation, fibrosis and endothelial dysfunction. In non-pregnant individuals with diabetes, similar vascular changes are attributed to disruptions in endothelial-to-mesenchymal transition (EndMT), a key process where endothelial cells adopt a mesenchymal phenotype. Here, we assess whether alterations in the fetoplacental macro- and microvasculature are attributed to EndMT, using human umbilical vein endothelial cells (HUVECs) and human term placental tissue, respectively. Transforming growth factor (TGF)- β 2 and interleukin (IL)-1 β induced morphological and molecular changes consistent with EndMT in both GDM and non-GDM HUVECs. The ability of TGF- β 2 and IL-1 β to alter expression of known EndMT regulators, *VWF*, *TGFBR1*, *IL1B* and *IL1R1*, was diminished in GDM HUVECs; however, all other hallmarks of EndMT were similar. In placental villous tissue, Slug and Snail, two key transcriptional regulators of EndMT, were detected in the villous stroma, suggesting that EndMT probably occurs in the placental microvasculature. We observed a reduction in endothelial marker genes *PECAM1*, *VWF* and *CDH5* in GDM placentas, suggesting reduced placental vascularisation. This was accompanied by a reduction in EndMT regulators *SNAI2*, *TGF2*, *TGFB3* and *TGFBR2*; however, there was no change in mesenchymal markers or other EndMT regulators. This suggests that there may be some alterations in EndMT in GDM but this probably does not fully explain the endothelial dysfunction and altered vascularisation that occurs in the fetoplacental vasculature in pregnancies complicated by GDM.

(Received 14 November 2024; first published online 30 March 2025)

Corresponding authors A. R. Byford and K. Forbes: Discovery and Translational Science Department, Leeds Institute of Cardiovascular and Metabolic Medicine, Faculty of Medicine and Health, University of Leeds, Leeds, LS2 9JT, UK. Email: a.r.byford@leeds.ac.uk, k.a.forbes@leeds.ac.uk

Key points

- Gestational diabetes mellitus (GDM) has been linked to altered placental vascularisation, fibrosis and endothelial dysfunction.
- Disruptions in endothelial-to-mesenchymal transition (EndMT), a process where endothelial cells adopt a mesenchymal phenotype, has been linked to vascular complications in diabetes, but EndMT in GDM has not been investigated.
- Transforming growth factor (TGF)- β 2 and interleukin (IL)-1 β induced morphological and molecular changes consistent with EndMT in GDM and non-GDM human umbilical vein endothelial cells (HUVECs). Although the expression of EndMT mediators, *VWF*, *TGFBR1*, *IL1B*, and *IL1R1*, was diminished in GDM HUVECs, other EndMT hallmarks were similar.
- Transcriptional regulators of EndMT, Slug and Snail, were detected in the human term placenta. Despite a reduction in endothelial markers, *PECAM1*, *VWF* and *CDH5*, as well as *SNAI2*, *TGFB2/3* and *TGFBR2* in GDM placenta, there was no change in mesenchymal or other EndMT markers.
- This suggests that, although there may be some changes to EndMT in GDM, the vascular dysfunction is probably not explained fully by alterations in EndMT.

Introduction

Gestational diabetes mellitus (GDM) is defined by hyperglycaemia with onset during pregnancy and its prevalence is increasing with an estimated 14% of pregnancies affected globally (Wang et al., 2022). Although this hyperglycaemia can be managed during pregnancy

and usually resolves postpartum, GDM has been linked to impaired fetal cardiac development and function, increased rates of congenital heart disease, and an increased risk of developing cardiometabolic diseases in adulthood (Aguilera et al., 2021; Al-Biltagi et al., 2021; Balsells et al., 2012; Chen et al., 2024; Depla et al., 2021;

Kramer et al., 2019; Liu et al., 2024; Venkataraman et al., 2016). Despite this, the underlying mechanisms of how GDM causes these effects in offspring is largely unknown. However, defects in fetal cardiac development and rates of long-term cardiovascular complications in offspring are linked to alterations in the fetoplacental vasculature, including endothelial dysfunction (Diniz et al., 2023).

In the human placenta, the microvasculature is comprised of the fetal capillaries residing in the chorionic villi, which function along with the trophoblast, to transfer nutrients, oxygen, and waste between the maternal and fetal circulation (Junaid et al., 2014; Wang & Zhao, 2010). The macrovasculature is comprised of the chorionic plate vessels and umbilical cord, which transport the nutrients, oxygen and waste between the placenta and fetus (Junaid et al., 2014; Wang & Zhao, 2010). Alterations in both the macro- and micro-fetoplacental vasculature have been reported in pregnancies complicated by GDM (Byford et al., 2021; Sobrevia et al., 2011). These reported alterations include villous immaturity (Daskalakis et al., 2008), altered vascularisation (Akarsu et al., 2017; Calderon et al., 2007; Daskalakis et al., 2008; Jirkovská et al., 2012; Stoz et al., 1988; Troncoso et al., 2017), fibrosis (Bhattacharjee et al., 2017; Ehlers et al., 2021), endothelial dysfunction (Wang et al., 2023; Zhou et al., 2016) and impaired endothelial barrier function (Cvitcic et al., 2018; Villota et al., 2021), which have also been linked to altered fetal heart development (Anbara et al., 2019; Diniz et al., 2023; Gordon et al., 2022). Therefore, understanding the mechanisms for placental vascular dysfunction in GDM is of clear importance.

Placental vascular development is dependent on vasculogenesis, where mesenchymal cells differentiate into endothelial cell and haematopoietic cell progenitors, forming angiogenic cell cords and eventually the primitive capillary network (Demir et al., 2007). Further expansion of the placental vascular network is dependent on angiogenesis, which requires both endothelial cell proliferation and migration (James et al., 2022). In other systems, this process is dynamic, and endothelial-to-mesenchymal transition (EndMT), the transdifferentiation process of endothelial cells towards

a mesenchymal phenotype (Piera-Velazquez & Jimenez, 2019), can occur. Cells undergoing EndMT have a more proliferative and migratory phenotype (Bischoff, 2019; Piera-Velazquez & Jimenez, 2019); thus, it is possible that EndMT could play a significant role in endothelial cell proliferation and migration in placental vascular development. Other hallmarks of EndMT include a change in morphology to elongated, spindle shaped cells, loss of cell junction molecules, such as VE-cadherin, loss of endothelial markers, and an increase in mesenchymal and myofibroblast markers, such as transgelin and alpha smooth muscle actin (α SMA) (Piera-Velazquez & Jimenez, 2019; Pinto et al., 2016). EndMT has been shown to be induced by members of the transforming growth factor (TGF)- β family, pro-inflammatory cytokines, such as interleukin (IL)-1 β , and microRNAs (miRNAs) (Pérez et al., 2017; Singh et al., 2024). In the canonical EndMT signalling pathway, TGF- β binds to heterodimeric TGF- β type I (TGF- β R1) and type II (TGF- β R2) receptor complex on the cell surface to induce phosphorylation of Smad proteins, which are then translocated to the nucleus, to activate the transcription factors, Snail and Slug, which in turn regulate the transcription of EndMT target genes (Singh et al., 2024).

EndMT was first described in the developing heart where it plays an essential role in valve formation and heart septation (Markwald et al., 1975, 1977), and disruptions in EndMT give rise to congenital heart defects (Anbara et al., 2019). More recently, Boss et al. (2023) have described EndMT in first-trimester placental endothelial cells, suggesting that EndMT may also play a key role in placental development, but this remains to be further explored. Given that EndMT is important during fetal heart development and is altered in congenital heart defects, and similar developmental processes occur in the developing fetal heart and placenta (Mahadevan et al., 2023), EndMT in the fetoplacental vasculature warrants further investigation.

Increasing evidence also indicates that EndMT is involved in disease processes, particularly in diabetes, where disrupted EndMT contributes to cardiovascular diseases and other vascular pathologies associated with

Abigail R. Byford, a postdoctoral researcher, and **Georgia Fakonti**, a final year PhD student, are members of Dr Karen Forbes and Prof Eleanor M. Scott's research groups in Leeds Institute of Cardiovascular and Metabolic Medicine (LICAMM) at the University of Leeds. Work in the Forbes group is focussed on understanding how factors in the maternal environment (primarily diet, microRNAs and extracellular vesicles) contribute to altered placental and fetal growth, and long-term health of the offspring, particularly in pregnancies complicated by maternal diabetes. Dr Karen Forbes has a programme of research spanning from understanding the basic mechanisms of disease progression, through to the development of potential novel therapeutics for prevention of these conditions. Dr Abigail R. Byford is investigating the link between maternal glucose and adverse outcomes in pregnancies complicated by maternal diabetes and Georgia Fakonti is investigating the molecular and cellular changes that contribute to placental dysfunction and adverse pregnancy outcomes in pregnancies complicated by maternal diabetes.



endothelial dysfunction and fibrosis (Kovacic et al., 2019; Wang, Wang, & Chakrabarti et al., 2023). It is therefore possible that exposure to a diabetic environment *in utero* also impacts EndMT, vascularisation, and associated processes in the developing placenta and fetus; however, to our knowledge, this has not been investigated. In the present study, we assess whether vascular dysfunction in the diabetic placenta could potentially be attributed to changes in EndMT. Using human umbilical cord endothelial cells (HUVECs) and placental villous tissue from GDM and non-GDM pregnancies we assess whether a diabetic environment *in utero* has the potential to influence EndMT in the fetoplacental macro- and micro-vasculature, respectively. We then assess whether a GDM environment alters EndMT by exposing both GDM and non-GDM HUVECs to known inducers of EndMT.

Methods

Placenta and umbilical cord collection and processing

Healthy pregnant women or women diagnosed with GDM, with singleton term deliveries (between 37 and 41 weeks of gestation) were recruited at the Leeds Teaching Hospital NHS trust (London – Riverside Research Ethics Committee; REC reference: 18/LO/0067; IRAS project ID: 234 385) or at St Mary's Hospital, Manchester University NHS Foundation Trust (Northwest Research Ethics Committee; REC reference: 08/H1010/55). All participants provide their written informed consent and all human tissue processing, data curation and analysis was conducted in accordance with the Declaration of Helsinki guidelines and the Human Tissue Act. GDM diagnosis was confirmed through an oral glucose tolerance test in women with risk factors as detailed within the National Institute of Clinical Excellence Diabetes in Pregnancy guideline (NICE, 2015). Either a fasting plasma glucose level of 5.6 mM or above or a 2 h post-prandial glucose level of 7.8 mM or above is diagnostic of GDM. In women with previous GDM, this would be conducted as soon as possible after booking and repeated at 24–28 weeks of gestation if the first was negative. In women with other risk factors for GDM, a single screening test was conducted at 24–28 weeks of gestation. Human term placentas and umbilical cords were collected within 30 min following delivery. Umbilical cords for HUVECs and placental tissue were processed from different patients. All umbilical cords were collected from Caesarean sections, and placentas were collected from both vaginal and Caesarean deliveries.

For processing of placental tissue, the fetal membranes and umbilical cord were removed, a sample of 5 cm² full thickness was collected from the centre (close to umbilical cord insertion), middle (between umbilical cord and edge) and edge of the placenta, representing the

entire organ. The samples were then washed with sterile phosphate-buffered saline (PBS) (Sigma-Aldrich, St Louis, MO, USA; catalog. no. D8537) to remove maternal blood. The basal and chorionic plates were then removed from each sample. For histology, a full thickness tissue section from the centre, middle and edge were stored in 10% neutral buffered formalin (NBF) (Sigma-Aldrich; catalog. no. HT501128) at 4°C. After 48 h, NBF was removed, replaced with 70% ethanol and stored at 4°C until the tissue was processed. For RNA, tissue pieces from the same centre, middle and edge samples were further dissected and small pieces from each area were pooled and placed in RNALater (Merck, Darmstadt, Germany; catalog. no. R0901-500ML) for 48 h, before being snap frozen in liquid nitrogen and stored at –80°C. Maternal demographic and pregnancy outcome information were recorded and birthweight centiles were calculated using the World Health Organisation fetal growth calculator (<https://srhr.org/fetalgrowthcalculator>), which considered gestational age, birthweight and fetal sex. Large-for-gestational age (LGA) infants were defined as a birthweight centile ≥ 90 .

HUVEC isolation

HUVECs were isolated from umbilical cords derived from non-GDM ($n = 6$) and GDM ($n = 5$) pregnancies. The umbilical cord was removed from the placenta and placed in sterile PBS (Gibco, Waltham, MA, USA; catalog. no. D8537). The umbilical vein was then cannulated and flushed with 20 mL of PBS to remove blood. Following this, 5 mL of 0.1% collagenase type II (Gibco; catalog. no. 17101-015) prepared in Hank's Buffer (Sigma-Aldrich; catalog. no. H9259) was flushed through the vein, and the end of the cord was clamped using a cord clamp, before filling with an additional 5 mL of collagenase. The cord was clamped at the other end and incubated for 20 min at 37°C. The lower cord clamp was removed and placed over a 50 mL falcon tube and flushed with 5 mL of Endothelial Cell Growth Medium 2 (EGM-2) (Promocell, Heidelberg, Germany; catalog. no. C22110), with 1% Antibiotic and Antimitotic (Gibco, catalog. no. 15240-062). The suspension was centrifuged for 6 min at 256 *g* and the supernatant removed. The pellet was then resuspended in 2 mL of EGM-2 and centrifuged again for 6 min at 256 *g*. This step was repeated twice, and the final pellet was resuspended in 5 mL of EGM-2 and plated into a T25 flask. Half of the medium was refreshed after 24 h and all the medium was refreshed after a further 48 h.

HUVEC cell culture

Primary HUVECs or commercial HUVECs (Promocell; catalog. no. C-12203, Lot #494Z025) (passages 2–6) were cultured in a humidified incubator at 37°C in 5% CO₂,

20% O₂ in EGM-2 with 1% Antibiotic and Antimitotic. HUVECs were passaged at 80–90% confluency using Accutase solution (Sigma-Aldrich; catalog. no. A6964 or Promocell; catalog. no. C-41310) and centrifuged at 220 *g* for 3 min. The supernatant was removed, and the cell pellet was resuspended in fresh EGM-2 before seeding. Medium was refreshed every 2–3 days.

Placental mesenchymal stromal cell (pMSC) culture

Placental mesenchymal stromal cells (pMSCs) were used as a mesenchymal cell positive control ($n = 7$; passages 2–6). Uncomplicated human term placentas were collected from the Leeds Teaching Hospital NHS trust (London – Riverside Research Ethics Committee; REC reference: 18/LO/0067; IRAS project ID: 234385) as described above. pMSCs were isolated and characterised as previously described (Kennedy, 2022; Pelekanos et al., 2016). Briefly, pMSCs were isolated using enzymatic digestion and were characterised using a human mesenchymal stem cell flow cytometry kit (R&D Systems, Minneapolis, MN, USA; catalog. no. FMC002) and tri-lineage differentiation (Kennedy, 2022). pMSCs were cultured in a humidified incubator at 37°C in 5% CO₂, 20% O₂ in low glucose Dulbecco's modified Eagle's medium (Gibco; catalog. no. 11885-092) supplemented with 10% fetal bovine serum (Gibco; catalog. no. 10270-106), 1% Antibiotic and Antimitotic (Gibco; catalog. no. 15240-062), and 1% Non-Essential Amino Acids (Gibco; catalog. no. 11140 035). pMSCs were passaged at 80–90% confluency using TryPLE Express (Gibco; catalog. no. 12563-029), which was inactivated with medium before seeding. Medium was refreshed every 2–3 days. pMSCs were seeded at 4000 cells cm² in either six-well plates, or in 24-well plates containing glass coverslips. On day 6, cells were washed with PBS and harvested for RNA isolation or fixed with 4% paraformaldehyde for 20 min followed by PBS washing for immunocytochemistry. Cells were imaged using an Oxion Inverso microscope (Euromex, Duiven, The Netherlands) with a 10× objective.

Confirmation of HUVEC purity using flow cytometry

HUVECs (passages 3–6) were characterised using flow cytometry. All centrifugation steps were performed at 220 *g* for 3 min. Once cells had reached 90–100% confluency they were removed from tissue culture flasks using Accutase solution (Sigma-Aldrich; catalog. no. A6964) and were centrifuged. The supernatant was removed, and the cell pellet was resuspended in 1 mL of staining buffer (R&D Systems; catalog. no. FC001), which contains bovine serum albumin (BSA) to minimise non-specific staining and the metabolic inhibitor

sodium azide as a preservative. In total, 100,000 cells were added to each tube. For blocking, 20 µL of Fc receptor blocking reagent, which blocks non-specific binding of antibodies to human Fc receptor-expressing cells (Miltenyi Biotec, Bergisch Gladbach, Germany; catalog. no. 130-059-901, RRID:AB_2 892112), was added to each tube and incubated for 10 min at 4°C. The cells were then centrifuged and incubated with the following fluorescence labelled antibodies: CD31-FITC (dilution 1:50; Miltenyi Biotec; catalog. no. 130-110-668, Lot #5240600353, RRID:AB_2657279) and CD144-PE (dilution 1:50; Miltenyi Biotec; catalog. no. 130-118-495, Lot #5240800873, RRID:AB_2751528) either alone (fluorescence minus one controls; FMOs) or in combination for 15 min at 4°C. An additional tube of cells in staining buffer without antibodies was used as an unstained control. Cells were then washed and resuspended in 200 µL of staining buffer for flow analysis using the Cytotflex S Flow Cytometer (Beckman, Brea, CA, USA). A gating strategy was applied to remove debris and doublets, and 10,000 events were recorded per tube.

Flow cytometry analysis was performed using CytExpert, version 2.4.0.28 (Beckman). Following debris and doublet exclusion, the percentage of cells expressing both CD31 and CD144 was measured, using the FMO control to aid gating (Fig. 1A).

EndMT induction in HUVECs

Other studies have used different methodologies to induce EndMT in endothelial cells, *in vitro*, including TGF-β1, TGF-β2 and IL-1β, either alone or in combination (Bronson et al., 2023; Chen et al., 2023; Ferreira et al., 2019; Maleszewska et al., 2013; Pinto et al., 2016; Terzuoli et al., 2020; Zhu et al., 2023). Therefore, to determine the best *in vitro* method to induce EndMT, commercial HUVECs were cultured in control medium (EGM-2 only) or EGM-2 containing either TGF-β1 (10 ng mL⁻¹; Merck; catalog. no. H8541-5UG), TGF-β2 (10 ng mL⁻¹; Biolegend, San Diego, CA, USA; catalog. no. 583301, Lot #B397313 and #B415636), TGF-β1 (10 ng mL⁻¹) with IL-1β (10 ng mL⁻¹; Biolegend; catalog. no. 579404, Lot #B398847) or TGF-β2 (10 ng mL⁻¹) with IL-1β (10 ng mL⁻¹) for 6 days ($n = 3$). Following initial optimisation of conditions for EndMT, further experiments were conducted using TGF-β2 (10 ng mL⁻¹) in combination with IL-1β (10 ng mL⁻¹) for 6 days ($n = 6$). For all EndMT experiments, medium was replenished every 1–3 days. Cells were seeded at 1000 cells cm² in either six-well plates, or in 24-well plates containing glass coverslips. On day 6, cells were washed with PBS and harvested for RNA isolation or fixed with 4% paraformaldehyde for 20 min followed by PBS washing for immunocytochemistry. Cells were imaged using an Oxion Inverso microscope (Euromex) with a 10× objective.

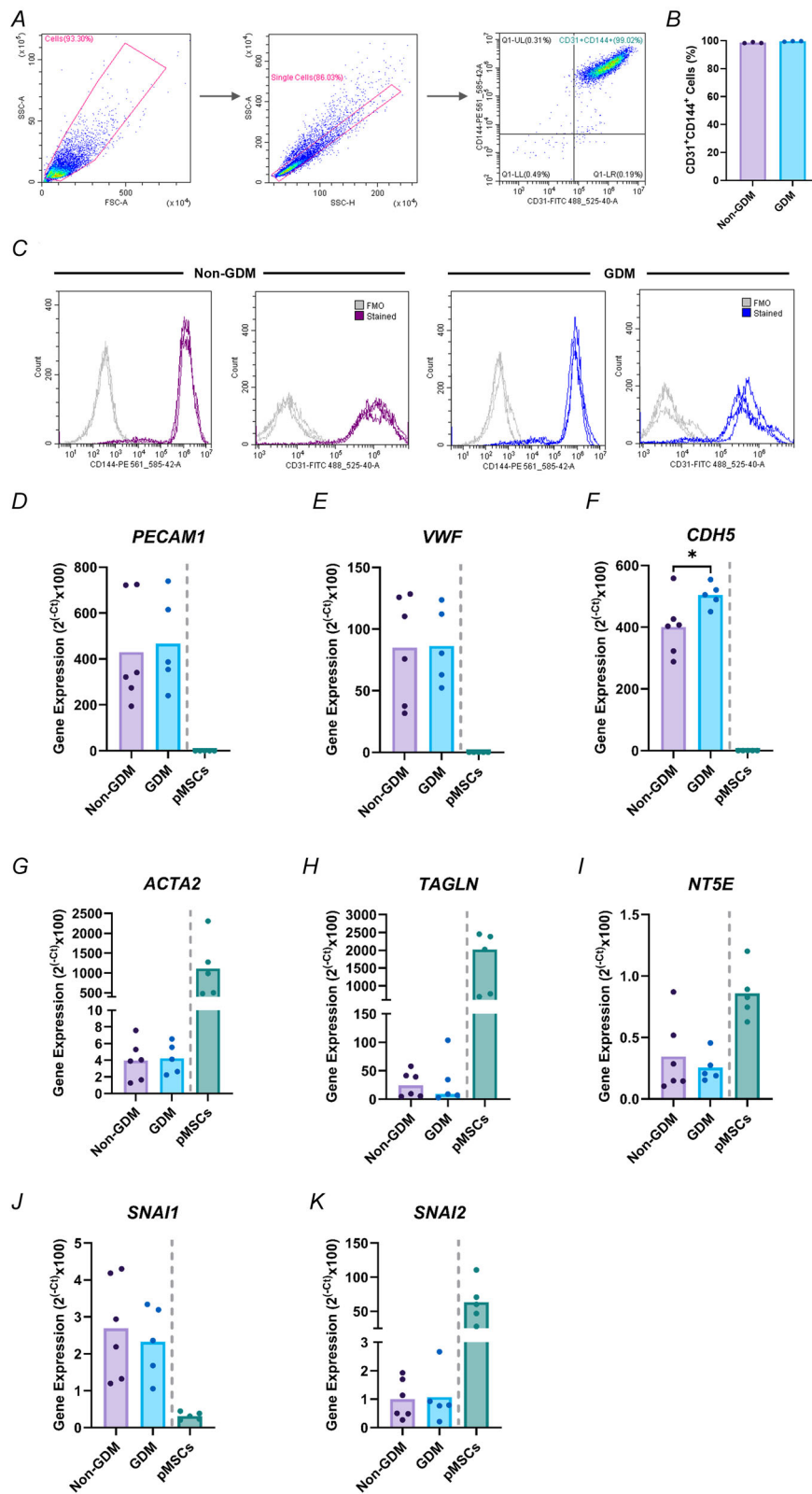


Figure 1.

A-C, characterisation of primary HUVECs from non-GDM and GDM pregnancies using flow cytometry. **A**, representative flow cytometry plots to demonstrate the gating strategy applied to remove debris and doublets. Representative flow cytometry plot to demonstrate the gating of CD31+CD144+ HUVECs. **B**, percentage of total HUVECs from non-GDM and GDM pregnancies, that co-express CD31 and CD144 ($n = 3$ per group). Data are presented as the mean. **C**, histograms of fluorescence minus one (FMO) controls and stained HUVECs from non-GDM and GDM pregnancies expressing CD144 and CD31 ($n = 3$ per group). **D-K**, expression of EndMT markers in non-GDM and GDM HUVECs. HUVECs were isolated from non-GDM ($n = 6$) and GDM pregnancies ($n = 5$) and expression of EndMT markers, including endothelial and mesenchymal markers, were measured via RT-qPCR. As a mesenchymal cell positive control, primary pMSCs were used. Data are presented as the mean. Statistical analysis was performed using an unpaired t test (normally distributed), except *TAGLN*, which is presented as the median and statistical analysis was performed using a Mann-Whitney U test (not normally distributed) (* $P < 0.05$ in GDM compared to non-GDM).

RNA isolation

For RNA isolation from HUVECs and pMSCs, cells were first washed with PBS. Total RNA was extracted (one-well of a six-well plate per condition/sample) using the miRNeasy Advanced Mini kit for tissues and cells (Qiagen, Hilden, Germany; catalog. no. 217604) in accordance with the manufacturer's instructions. This included a gDNA eliminator spin column to remove potential contaminating gDNA. All centrifugation steps were performed at 12,000 *g*, except for the final steps to dry the membrane and elute RNA, which were performed at maximum speed. RNA was eluted in 40 μ L of nuclease-free water and stored at -80°C .

For RNA isolation from human term placental tissue, total RNA was isolated using the mirVana™ miRNA isolation kit (Thermo Fisher Scientific, Waltham, MA, USA; catalog. no. AM1561) in accordance with the manufacturer's instructions. Briefly, 0.25 g of snap frozen tissue was lysed and homogenised using 300 μ L of lysis/binding buffer and 30 μ L of miRNA homogenate additive. Phase separation was performed using 300 μ L of acid-phenol:chloroform (Ambion, Austin, TX, USA; catalog. no. AM9720). All centrifugation steps were performed at 10,000 *g* except for elution, which was performed at maximum speed in 100 μ L of pre-heated (95°C) nuclease-free water. The recovered RNA was then purified using the RNA clean and concentrator-5 kit (Zymo Research, Irvine, CA, USA; catalog. no. R1014) in accordance with the manufacturer's instructions. To remove potential contaminating gDNA, 40 μ L of isolated RNA was incubated with 5 μ L of Dnase I and 5 μ L of DNA Digestion Buffer for 15 min at room temperature. All centrifugation steps were performed at 10,000 *g*. RNA was eluted in 15 μ L of nuclease-free water and stored at -80°C .

For all RNA samples, concentration and quality (260:280 and 260:230 ratios) were assessed using a NanoDrop spectrophotometer (DeNovix, Wilmington, DE, USA; DS-11).

Quantitative reverse transcriptase PCR (RT-qPCR)

RT-qPCR was used to measure gene expression. For complementary DNA (cDNA) synthesis, the Affinity Script Multiple Temperature cDNA Synthesis Kit (Agilent, Santa Clara, CA, USA; catalog. no. 200436) was used in accordance with the manufacturer's instructions. Samples were prepared by adding 100 ng RNA to nuclease-free water in a total volume of 12.5 μ L. No template and no reverse transcriptase controls were also prepared with nuclease-free water to replace the RNA or the reverse transcriptase enzyme, respectively. Samples were placed in a thermal cycler (Applied Biosystems Venti 96 Well; Thermo Fisher Scientific) and were heated to 25°C for

10 min, 42°C for 60 min and 70°C for 15 min, with a final indefinite hold at 4°C . Samples were stored at -20°C .

RT-qPCR was conducted using specific primers at a final concentration of 0.36 μM (Table 1) and the Brilliant III Ultra-Fast SYBR Green Master Mix kit (Agilent; catalog. no. 600882) in accordance with the manufacturer's instructions. cDNA was diluted 1:10. Samples were loaded in duplicate into white-bottom qPCR plates. Plates were loaded into a LightCycler 96 Instrument (Roche, Basel, Switzerland). Plates were pre-incubated at 95°C for 3 min, followed by 40 cycles of two-step amplification: 95°C for 20 s, then a primer specific annealing step (Table 1) for 20 s. This was followed by a final cycle of 95°C for 1 min, 55°C for 30 s and 95°C for 1 s to generate dissociation curves to confirm the PCR product. The data were then analysed using the LightCycler 96 1.1 software (Roche). Data were acquired as an amplification curve and raw cycle threshold (C_t) values which were used to calculate the relative gene expression via the $2^{-(C_t)} \times 100$ method, normalising against the housekeeping gene *YWHAZ*.

Immunocytochemistry and fluorescence microscopy

For intracellular staining, cells cultured on coverslips were permeabilised with PBS containing 0.1% Triton-X100 (Sigma-Aldrich; catalog. no. X100-500ML) for 30 min. Coverslips were then washed three times with PBS and blocked with 5% BSA (Roche; catalog. no. 10735078001) in PBS for 30 min at room temperature. Following blocking, cells were incubated with primary antibodies diluted in 5% BSA, specific for endothelial and mesenchymal markers, EndMT regulators and proliferative markers (Table 2) overnight at 4°C . After incubation, coverslips were washed three times with PBS to remove unbound primary antibody and were incubated with appropriate fluorescence labelled secondary antibodies, diluted in 5% BSA (Table 2) for 1.5 h at room temperature. Coverslips were then washed three times with PBS to remove unbound secondary antibody and were then mounted onto fresh microscope slides using Fluoromount-G with 4',6-diamidino-2-phenylindole (DAPI) (Southern Biotech, Birmingham, AL, USA; catalog. no. 0100-20). Negative controls included coverslips incubated with an isotype-specific control or with secondary antibody only.

Visualisation and imaging of coverslips was performed using an IX83 microscope (Olympus, Tokyo, Japan) with a $20\times/0.75$ U PlanS Apo objective. For each coverslip, three regions of interest (ROI) were imaged. The same exposure times were used for each antibody across all samples. Images were analysed using QuPath, version 0.5.1 (<https://qupath.github.io>), comprising software for digital bioimage analysis (Bankhead et al., 2017). Firstly,

Table 1. Primers used for RT-qPCR.

Gene name	Primer	Sequence (5' to 3')	Annealing Temperature (°C)	Product length	Reference
ACTA2 (α SMA)	Forward primer	TGAGCGTGGCTATTCCTTCGT	65	108	Designed
	Reverse primer	GCAGTGGCCATCTCATTTTCAA			
ACVRL1 (ALK1)	Forward primer	TGCAGTGTTCATCGCCGAC	62	269	Designed
	Reverse primer	TGGGGTCATTGGGCACCACA			
CDH5 (VE-cadherin)	Forward primer	CAGGCAGTCCAACGGAACAGAAA	60	863	Designed
	Reverse primer	CGACAAATGTGTACTTGGTCTGGGT			
IL1B	Forward primer	CACCAATGCCCAACTGCCTGC	60	219	Designed
	Reverse primer	TGCTCATCAGAATGTGGGAGCGA			
IL1R1	Forward primer	AGAGGAAAAACAAACCCACAAGG	55	106	(Bellehumeur et al., 2009)
	Reverse primer	CTGGCCGGTGACATTACAGAT			
NT5E (CD73)	Forward primer	CTAGCGCAACCACAAACCATAC	65	79	Designed
	Reverse primer	CTGGGTCCTCTCTGAGTCTCG			
PECAM1 (CD31)	Forward primer	GCTGAGTCTCACAAGATCTAGGA	57	91	(Böhrnsen & Schliephake, 2016)
	Reverse primer	ATCTGCTTCCACGGCATCA			
SMAD2	Forward primer	GGAGCAGAATACCGAAGGCA	60	128	(Yu et al., 2009)
	Reverse primer	CTTGAGCAACGCACTGAAGG			
SMAD3	Forward primer	AGAAGACGGGGCAGCTGGAC	60	511	(Yu et al., 2009)
	Reverse primer	GACATCGGATTCGGGGATAG			
SMAD4	Forward primer	GCATCGACAGAGACATACAG	60	411	(Yu et al., 2009)
	Reverse primer	CAACAGTAACAATAGGGCAG			
SNAI1 (Snail)	Forward primer	CTTCAGCAGCCCTACGAC	60	71	(Terzuoli et al., 2020)
	Reverse primer	CGGTGGGGTTGAGGATCT			
SNAI2 (Slug)	Forward primer	ACTCCGAAGCCAAATGACAA	60	119	(Xu et al., 2015)
	Reverse primer	CTCTCTGTGGGTGTGTGT			
TAGLN (Transgelin)	Forward primer	GGCTGAAGAATGGCGTGATT	60	108	Designed
	Reverse primer	TCTGCTTGAAGACCATGGAGG			
TGFB1	Forward primer	GGTTGAGCCGTGGAGGGGAAAT	60	280	Designed
	Reverse primer	ATGTACAGCTGCCGCACGCA			
TGFB2	Forward primer	GTTGATTGACGTCTCAGCAAT	60	112	(Yoshimatsu et al., 2020)
	Reverse primer	CAATCCGTTGTCAGGCACTCT			
TGFB3	Forward primer	ATGACCCACGTCCCCTATCA	60	113	(Yoshimatsu et al., 2020)
	Reverse primer	TCCGACTCGGTGTTTCTCTG			
TGFB1 (ALK5)	Forward primer	AACTTGCTCTGTCCACGGCG	60	238	Designed
	Reverse primer	ACTTCAGGGGCCATGTACCTTT			
TGFB2	Forward primer	TGGCTCAACCACCAGGGCAT	60	96	Designed
	Reverse primer	TGCCACACACTGGGCTGTGA			
VWF	Forward primer	CCCATTGCTGAGCCTTGT	57	141	(Wang et al., 2018)
	Reverse primer	GGATGACCACCGCCTTTG			
YWHAZ	Forward primer	ACTTTTGGTACATTGTGGCTTCAA	55	94	Designed
	Reverse primer	CCGCCAGGACAAACCATAT			

the brightness and contrast settings for each channel were adjusted and applied across all images. A pixel classifier threshold was set to detect the cells in each ROI. The fluorescence intensity was then determined using the intensity features tool. The intensity was calculated per pixel, to account for differing numbers and sizes of cells in each ROI/image. To measure proliferation, the positive cell detection tool was used to identify all DAPI-positive and Ki67-positive cells and the percentage of Ki67 positive cells was then calculated.

Immunohistochemistry

Following fixation in 10% NBF, human placental tissue was dehydrated and cleared using a tissue processor (Lecia, Wetzlar, Germany; TP1020) and embedded in paraffin wax. Formalin-fixed paraffin-embedded tissue was then cut into 5 μ m sections using a microtome (Lecia; RM2125RTF) and transferred onto poly-L-lysine coated slides (VWR, Radnor, PA, USA; catalog. no. 631-0107). Tissue sections were dewaxed and rehydrated using

Table 2. Antibodies used for immunocytochemistry and/or immunohistochemistry.

Protein	Labels	Host	Stock Concentration	Dilution	Final Concentration	Manufacturer	Catalog. no.	Lot #; RRID
CD31	Endothelial	Mouse	201 $\mu\text{g mL}^{-1}$	1:100	2.01 $\mu\text{g mL}^{-1}$	Dako	M0823	41 526 059; RRID:AB_2 114 471
VWF	Endothelial	Mouse	140 $\mu\text{g mL}^{-1}$	1:200	0.7 $\mu\text{g mL}^{-1}$	Dako	M0616	20 084 172; RRID:AB_2 216 702
VE-Cadherin	Endothelial	Rabbit	105 $\mu\text{g mL}^{-1}$	1:600	0.175 $\mu\text{g mL}^{-1}$	Cell Signaling Technologies	2500	5; RRID:AB_10 839 118
Transgelin	Mesenchymal	Rabbit	900 $\mu\text{g mL}^{-1}$	1:300	3 $\mu\text{g mL}^{-1}$	Abcam	ab14106	GR3438803-1; RRID:AB_443 021
αSMA	Mesenchymal	Mouse	1000 $\mu\text{g mL}^{-1}$	1:80	12.5 $\mu\text{g mL}^{-1}$	R&D Systems	MAB1420	IBR0922071; RRID:AB_262 054
Ki67	Proliferation	Mouse	46 $\mu\text{g mL}^{-1}$	1:50	0.92 $\mu\text{g mL}^{-1}$	Dako	M7240	20 075 742; RRID:AB_2 142 367
Snail	Transcription factor	Mouse	200 $\mu\text{g mL}^{-1}$	1:100	2 $\mu\text{g mL}^{-1}$	Santa Cruz	SC-271 977	K0520; RRID:AB_10 709 902
Slug	Transcription factor	Mouse	200 $\mu\text{g mL}^{-1}$	1:100	2 $\mu\text{g mL}^{-1}$	Santa Cruz	SC-166 476	A1518; RRID:AB_2 191 897
Mouse IgG	Isotype control	Mouse	2000 $\mu\text{g mL}^{-1}$	Various	Various	Vector Labs	I-2000-1	ZG0115; RRID:AB_2 336 354
Rabbit IgG	Isotype control	Rabbit	5000 $\mu\text{g mL}^{-1}$	Various	Various	Vector Labs	I-1000-5	ZH1201; RRID:AB_2 336 355
Anti-mouse 488	Secondary	Goat	2000 $\mu\text{g mL}^{-1}$	1:2000	1 $\mu\text{g mL}^{-1}$	Thermo Fisher Scientific	A11001	2 090 562; RRID:AB_2 534 069
Anti-rabbit 488	Secondary	Goat	2000 $\mu\text{g mL}^{-1}$	1:2000	1 $\mu\text{g mL}^{-1}$	Thermo Fisher Scientific	A11008	2 051 237; RRID:AB_143 165
Anti-mouse 568	Secondary	Goat	2000 $\mu\text{g mL}^{-1}$	1:1500	1.3 $\mu\text{g mL}^{-1}$	Thermo Fisher Scientific	A11031	2 026 148; RRID:AB_144 696
Anti-rabbit 568	Secondary	Goat	2000 $\mu\text{g mL}^{-1}$	1:1500	1.3 $\mu\text{g mL}^{-1}$	Thermo Fisher Scientific	A11011	54936A; RRID:AB_143 157
Anti-mouse biotin	Secondary	Goat	1000 $\mu\text{g mL}^{-1}$	1:200	5 $\mu\text{g mL}^{-1}$	AAT Bioquest	16 729	2 760 781;C RRID:AB_3 665 168
Anti-rabbit biotin	Secondary	Swine	510 $\mu\text{g mL}^{-1}$	1:200	2.55 $\mu\text{g mL}^{-1}$	Dako	E0353	20 016 769; RRID:AB_2 737 292

Table 3. Maternal and fetal demographic information for HUVEC samples used.

	Non-GDM (<i>n</i> = 6)	GDM (<i>n</i> = 5)	<i>P</i> value
Maternal age (years)¹	28.8 ± 4.83	32.4 ± 3.51	0.204
Booking BMI (kg m²)¹	23.9 ± 4.20	34.7 ± 8.33	0.0204
Ethnicity²	Chinese = 1; White British = 4, Indian = 1	African = 1; Indian = 1, Asian (other) = 1; White British = 2	0.740
Gestational age (days)¹	274.0 ± 1.67	270.6 ± 3.78	0.0770
Parity²	P0 = 3 P1 = 2 P2 = 1	P0 = 1 P1 = 1 P2 = 1 P3 = 2	0.584
Placental weight (g)¹	403.0 ± 53.0	534.0 ± 47.2	0.00210
Birthweight (g)¹	3335 ± 338.6	3615 ± 262.8	0.167
Birthweight centile¹	42.42 ± 25.50	73.56 ± 20.19	0.0546
Birthweight class²	AGA = 6	LGA = 1; AGA = 4	0.455
Fetal sex²	Male = 3; female = 3	Male = 2; female = 3	1.00
GDM medication²	NA	Metformin = 1; insulin and metformin = 2; not available = 2 ^a	NA

Data are presented as the ¹mean ± standard deviation and ²absolute numbers. Statistical analysis was performed using an unpaired *t* test (maternal age, booking BMI, gestational age, placental weight, birthweight; normally distributed continuous data) or a Fisher's exact test (ethnicity, parity, birthweight class, fetal sex; categorical data). Abbreviations: LGA, large for gestational age; AGA, appropriately grown for gestational age; BMI, body mass index; NA, not applicable. ^aNot available (either no medication is prescribed, or no medication was identified in the medical records and available demographics). All HUVECs were isolated from elective Caesarean section deliveries.

HistoClear (National Diagnostics, Atlanta, GA, USA; catalog. no. NAT1330) and decreasing concentrations of ethanol (from 100% to 70%). Heat-activated antigen retrieval was performed by boiling tissue in 0.01 M sodium citrate buffer (pH 6.0). Immunohistochemistry was performed using specific antibodies for endothelial and mesenchymal markers and EndMT regulators (Table 2), which were incubated overnight at 4°C. After incubation, slides were washed three times with Tris-buffered saline to remove unbound primary antibody and were incubated with appropriate biotinylated secondary antibodies (Table 2), for 1 h at room temperature and immunoreactivity was visualised using the avidin-peroxidase method followed by 3,3'-diaminobenzidine (i.e. DAB) as previously described (Forbes et al., 2008). Sections were counterstained with haematoxylin (Sigma-Aldrich; catalog. no. HHS16) then dehydrated and cleared in HistoClear before mounting with coverslips using DPX (Thermo Fisher Scientific). Sections were imaged using the Axioscan Z1 Slide Scanner (Zeiss).

Statistical analysis

Statistical analysis was performed using Prism, version 10.2.0 (GraphPad Software Inc., San Diego, CA, USA). Data were assessed for normality using quantile-quantile plots and Shapiro-Wilk tests. When continuous data

were normally distributed, an unpaired *t* test or one-way analysis of variance (ANOVA) followed by Dunnett's *post hoc* test was used. When continuous data were not normally distributed, the Mann-Whitney *U* test or Kruskal-Wallis test followed by Dunn's *post hoc* test was used. For grouped data, a two-way ANOVA was performed with Fisher's *post hoc* test. Grouped data that were not normally distributed were log transformed and assessed using a two-way ANOVA. For categorical data, Fisher's exact test was used. *P* < 0.05 was considered statistically significant.

Results

EndMT markers are expressed in HUVECs

To investigate whether GDM could potentially exert changes to EndMT we first isolated HUVECs from non-GDM (*n* = 6) and GDM pregnancies (*n* = 5) (Table 3) and assessed the expression of EndMT markers. The phenotype of the HUVECs was confirmed using flow cytometry (*n* = 3 per group) which demonstrated that the isolated cells from both non-GDM and GDM pregnancies co-expressed CD31 and VE-cadherin/CD144 (98.57 ± 0.40% and 99.59 ± 0.24%, respectively) (Fig. 1A-C), confirming their endothelial phenotype. RT-qPCR demonstrated that, as expected, HUVECs expressed the endothelial genes *PECAM1* (CD31), *VWF* and *CDH5*

(VE-cadherin) (Fig. 1D–F). There was minimal gene expression of mesenchymal markers, *ACTA2* (α SMA), *TAGLN* (transgelin), and *NT5E* (CD73) compared to isolated pMSCs (Fig. 1G–I). EndMT transcription factors, *SNAIL1* (Snail) and *SNAIL2* (Slug), were also expressed at low levels in HUVECs (Fig. 1J–K). No differences were observed in expression of mesenchymal markers, EndMT transcription factors, or the majority of endothelial markers, between GDM and non-GDM HUVECs, except for *CDH5* which was higher in GDM HUVECs ($P = 0.0486$) (Fig. 1F).

EndMT potential in HUVECs from GDM and non-GDM pregnancies

Next, we assessed whether there is altered EndMT potential in HUVECs from pregnancies complicated by GDM. First, initial experiments were performed to determine the best method for inducing EndMT in HUVECs (Fig. 2) and it was established that the combination of TGF- β 2 and IL-1 β was optimal for EndMT induction in commercial HUVECs (Fig. 2), consistent with previous studies (Maleszewska et al., 2013). We then assessed whether there were differences between TGF- β 2 and IL-1 β EndMT induction in HUVECs isolated from GDM and non-GDM pregnancies. Treatment of non-GDM HUVECs with TGF- β 2 and IL-1 β induced morphological changes consistent with EndMT, where cells were more elongated and spindle-shaped (Fig. 3A). This was accompanied by reduced expression of endothelial genes *PECAM1* ($P = 0.00140$), *VWF* ($P < 0.001$) and *CDH5* ($P < 0.001$) (Fig. 3B–D) and increased expression of mesenchymal genes *TAGLN* ($P < 0.0001$) and *NT5E* ($P < 0.001$) (Fig. 3F–G). Analysis of immunocytochemistry images (Fig. 3H–M and N) demonstrated that treatment exerted similar changes to endothelial and mesenchymal markers in HUVECs from non-GDM pregnancies at the protein level. Specifically, there was reduced protein expression of CD31 ($P = 0.0206$), VE-Cadherin ($P < 0.001$), and VWF ($P < 0.001$) (Fig. 3H–J and N) and increased levels of transgelin ($P < 0.0001$) (Fig. 3L and N). Interestingly, there was no change in *ACTA2* levels (Fig. 3E) following treatment, but there was a reduction in α SMA protein expression ($P = 0.0392$) (Fig. 3K). Proliferation of HUVECs was also assessed using Ki67, revealing that EndMT induction in HUVECs reduced the percentage of Ki67 positive cells ($12.25 \pm 12.25\%$ compared to $72.29 \pm 20.53\%$, $P < 0.0001$) (Fig. 3M and N).

In GDM HUVECs, TGF- β 2, and IL-1 β exposure also induced EndMT (Fig. 3). Although cell morphology, (Fig. 3A), levels of most endothelial and mesenchymal genes (Fig. 3B–G) and proteins (Fig. 3H–M and N) and rates of proliferation (Ki67; Fig. 3M and N) were

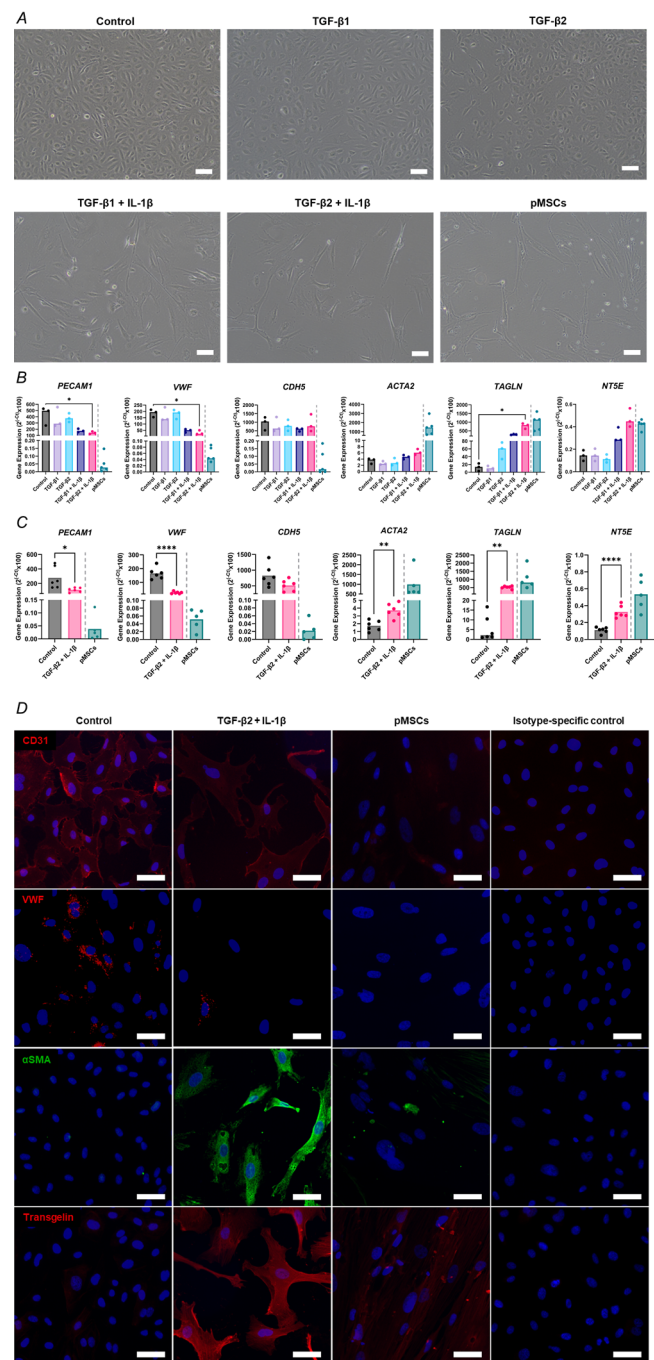


Figure 2. A combination of TGF- β 2 and IL-1 β is optimal for induction of EndMT in HUVECs

HUVECs (Promocell) were cultured in either control medium (EGM-2 only) or treated with EGM-2 containing TGF- β 1 (10 ng mL^{-1}), TGF- β 2 (10 ng mL^{-1}), TGF- β 1 (10 ng mL^{-1}) with IL-1 β (10 ng mL^{-1}) or TGF- β 2 (10 ng mL^{-1}) with IL-1 β (10 ng mL^{-1}) for 6 days ($n = 3$). As a mesenchymal cell positive control, primary pMSCs were used. A, morphological images of HUVECs captured using an Euromex Oxion Inverso microscope $10\times$ magnification. Scale bars = $100 \mu\text{m}$. B, expression of endothelial and mesenchymal genes measured via RT-qPCR. Data are presented as the median. Statistical analysis was performed using a Kruskal–Wallis with a Dunn's *post hoc* test between control and treated HUVECs ($*P < 0.05$). C, further HUVECs (Promocell) were cultured in either control medium (EGM-2

only) or treated with EGM-2 containing TGF- β 2 (10 ng mL⁻¹) and IL-1 β (10 ng mL⁻¹) for 6 days. As a mesenchymal cell positive control primary placental mesenchymal stromal cells (pMSCs) were used. Gene expression of endothelial and mesenchymal genes measured via RT-qPCR ($n = 6$). Data is presented as the mean. Statistical analysis was performed using an unpaired t test between control and treated HUVECs (normally distributed), except *TAGLN*, which is presented as the median and statistical analysis was performed using a Mann–Whitney U test (not normally distributed; * $P < 0.05$, ** $P < 0.01$, *** $P < 0.001$, **** $P < 0.0001$). **D**, immunocytochemistry of HUVECs ($n = 3$) and pMSCs stained with CD31, VWF, α SMA and transgelin, imaged using an Olympus IX83 microscope at 20 \times magnification. Scale bars = 50 μ m. Isotype-specific controls were also used. The same exposure times were used for each antibody across all samples. Further image processing was performed in Qupath, version 0.5.1, including adjustments for brightness and contrast, where the same settings were for each antibody across all samples.

comparable with treated non-GDM HUVECs, there were some subtle differences between the groups. Expression of *CDH5* was significantly higher in treated GDM HUVECs than in non-GDM HUVECs ($P = 0.00790$) (Fig. 3D); however, this is probably attributed to higher basal levels of *CDH5* in GDM HUVECs (Fig. 1F) because there was no difference in degree of induction by TGF- β 2 and IL-1 β (fold change compared to control) in *CDH5* gene expression or in VE-cadherin protein expression, which is encoded by the *CDH5* gene in GDM HUVECs (Fig. 3J and N). Interestingly, when we analysed the data (Fig. 3B–G) by assessing the fold change, *VWF* gene expression following treatment was lower in GDM compared to non-GDM ($P = 0.0384$), suggesting that the induction of EndMT may have less of an impact on *VWF* expression in GDM HUVECs.

Regulators of EndMT are altered in HUVECs from pregnancies complicated by GDM

We next assessed the impact of GDM on expression of key EndMT regulatory molecules in HUVECs. No differences in *TGFB1* (Fig. 4A), *TGFB3* (Fig. 4C), *ACVRL1* (ALK1) (Fig. 4E), *SMAD2* (Fig. 4K) or *SMAD4* (Fig. 4M) were observed between GDM and non-GDM HUVECs whether untreated or following EndMT induction. In both GDM and non-GDM HUVECs, EndMT induction resulted in a reduction in TGF β Receptor 2 (*TGFB2*; non-GDM: $P = 0.00700$, GDM: $P = 0.0220$) (Fig. 4F) and *SMAD3* (non-GDM: $P = 0.0163$; GDM: $P = 0.0152$) (Fig. 4L) following TGF- β 2 and IL-1 β treatment. This was accompanied by increased expression of *TGFB2* (non-GDM: $P < 0.0001$; GDM: $P < 0.0001$) (Fig. 4B), TGF- β receptor 1 (*TGFB1*)/activin receptor-like kinase 5 (ALK5; non-GDM: $P < 0.0001$, GDM: $P < 0.0001$) (Fig. 4D), *SNAIL1* (non-GDM: $P = 0.0107$; GDM: $P < 0.001$) (Fig. 4I) and *SNAIL2* (non-GDM: $P = 0.0191$;

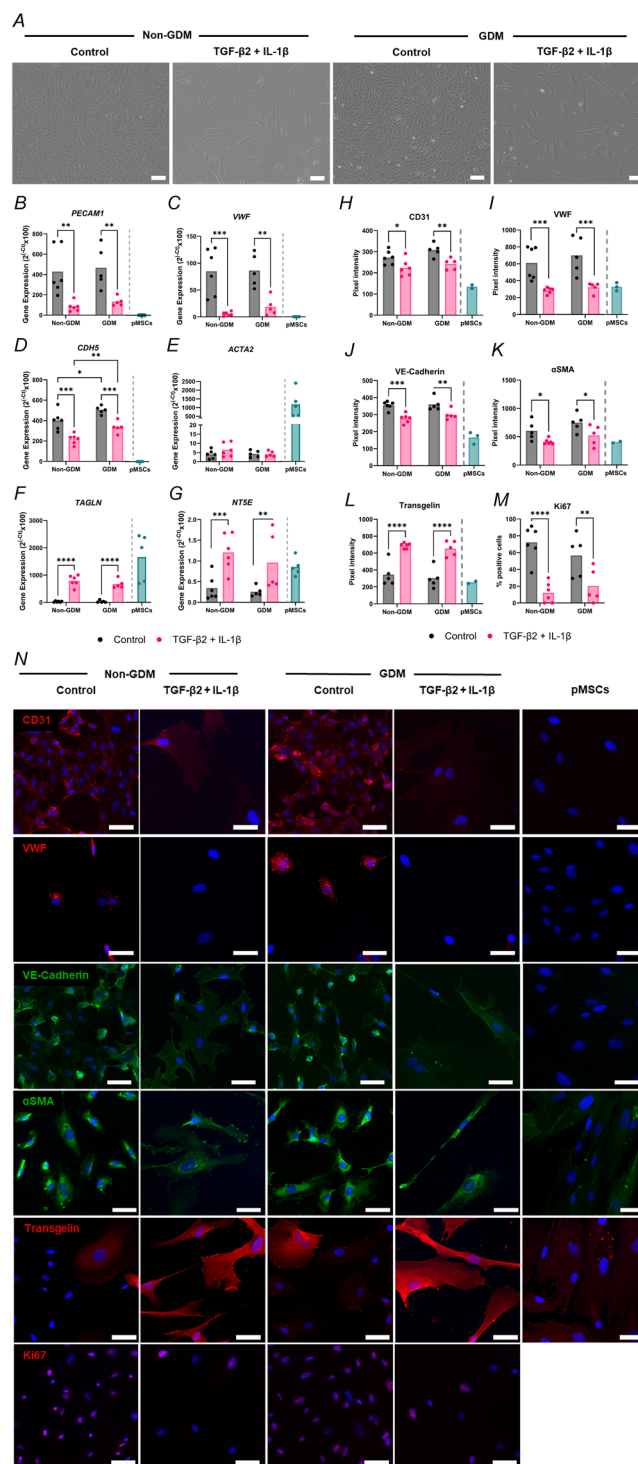


Figure 3. EndMT can be induced in primary HUVECs from non-GDM and GDM pregnancies

HUVECs isolated from non-GDM ($n = 6$) and GDM pregnancies ($n = 5$) were cultured in either control medium (EGM-2 only) or treated with EGM-2 containing of TGF- β 2 (10 ng mL⁻¹) and IL-1 β (10 ng mL⁻¹) for 6 days. As a mesenchymal cell positive control primary pMSCs were used. **A**, morphological images of HUVECs captured using an Euromex Oxion Inverso microscope at 10 \times

magnification. Scale bars = 100 μ m. *B–G*, expression of endothelial and mesenchymal genes measured via RT-qPCR. Data is presented as the mean. Statistical analysis was performed using two-way ANOVA with a Fisher's *post hoc* test (data that were not normally distributed were log-transformed; * $P < 0.05$, ** $P < 0.01$, *** $P < 0.001$, **** $P < 0.0001$). *H–N*, immunocytochemistry of HUVECs and pMSCs stained with CD31, VWF, VE-cadherin, α SMA, transgelin and Ki67, imaged using the Olympus IX83 microscope at 20 \times magnification. The same exposure times were used for each antibody across all samples. Further image processing and quantification was performed in Qupath, version 0.5.1), including adjustments for brightness and contrast, where the same settings were for each antibody across all samples. A pixel classifier threshold was set to detect the cells in each ROI. The fluorescence intensity was then determined using the intensity features tool. The intensity was calculated per pixel, to account for differing numbers and sizes of cells in each ROI/image. For Ki67 analysis, the positive cell detection tool was used to identify total DAPI positive cells and Ki67 positive cells. pMSCs were not included in Ki67 analysis because they were used as a mesenchymal cell positive control and, because these were cultured over different time periods, they were not needed for comparison for levels of proliferation. Quantification data (*H–M*) are presented as the mean. Statistical analysis was performed using two-way ANOVA with a Fisher's *post hoc* test (data that were not normally distributed were log-transformed; * $P < 0.05$, ** $P < 0.01$, *** $P < 0.001$, **** $P < 0.0001$). Representative images are shown in (*N*). Scale bars = 50 μ m.

GDM: $P < 0.001$) (Fig. 4J). EndMT induction of *TGFBR1* expression was lower in GDM HUVECs compared to non-GDM HUVECs ($P < 0.001$) (Fig. 4D). TGF- β 2 and IL-1 β increased levels of *IL1B* (Fig. 4G) and *IL1R* (Fig. 4H) expression only in non-GDM HUVECs ($P = 0.0160$ and $P = 0.00630$, respectively), with no change in GDM HUVECs. This suggests that a GDM environment may impact the regulatory mechanisms controlling EndMT in HUVECs.

EndMT markers are expressed in human placental villous tissue

To determine whether GDM has the potential to impact EndMT in placental microvascular endothelial cells, we performed immunohistochemistry for EndMT transcription factors, Snail and Slug, along with endothelial (CD31) and mesenchymal markers (transgelin and α SMA) (Fig. 5A) in term human placental tissue obtained from GDM and non-GDM pregnancies. As expected, CD31 was localised to the endothelium of placental blood vessels (Fig. 5A) and transgelin and α SMA were detected in both villous stroma and placental blood vessels. Snail was detected in the villous stroma in both GDM and non-GDM placenta (Fig. 5A), whereas Slug was present in trophoblast and villous stroma, particularly surrounding placental vessels, in both non-GDM and GDM placenta (Fig. 5A).

We next assessed whether a GDM environment had the potential to influence EndMT in the placenta in term human placental lysates from non-GDM and GDM pregnancies (Table 4) by assessing expression of EndMT markers and mediators; however, the levels of *NT5E*, *SMAD3*, and *IL1B* were at the lower end of detection, and so it was not possible to assess whether they were altered between groups. In the GDM placenta, there was a down-regulation of endothelial markers *PECAM1* ($P = 0.00600$), *VWF* ($P < 0.001$) and *CDH5* ($P = 0.0373$) (Fig. 5B–D), as well as downregulation of *SNAI2* ($P = 0.0121$) (Fig. 5O), *TGFB2* ($P = 0.00390$) (Fig. 5H), *TGFB3* ($P = 0.00270$) (Fig. 5I) and *TGFB2* ($P = 0.0487$) (Fig. 5L) indicating that there may be less EndMT occurring in the GDM placentas. However, when we assessed levels of mesenchymal markers, *TAGLN* and *ACTA2* (Fig. 5E and F), as well as other EndMT mediators (Fig. 5G–Q), there were no differences. All of this taken together suggests that there is reduced vascularisation in the GDM placentas, which is not a result of elevated EndMT.

Discussion

GDM increases the risk of pregnancy complications and is associated with alterations in the fetoplacental micro- and macrovasculature (Byford et al., 2021; Sobrevia et al., 2011). Here, we show that EndMT regulatory markers are present in both the micro- and macrovasculature of the placenta in non-GDM and GDM pregnancies. Although the potential for EndMT induction is not altered in the macrovasculature in GDM, subtle alterations in EndMT regulatory genes occur in the microvasculature.

Induction of EndMT has been widely reported in HUVECs (Bronson et al., 2023; Chen et al., 2023; Ferreira et al., 2019; Maleszewska et al., 2013; Terzuoli et al., 2020) and, more recently, EndMT was described in first trimester placental endothelial cells, suggesting that EndMT may contribute to placental vascular development and function (Boss et al., 2023). As far as we are aware, we are the first to show that EndMT mediators (Snail and Slug) are present in the villous stroma in term human placenta. This suggests that EndMT probably plays a role in maintenance of tissue homeostasis in the placenta and, given other documented roles for EndMT, this could probably involve the development and function of placental vessels (Piera-Velazquez & Jimenez, 2019). Boss et al. (2023) also demonstrated that first trimester placental endothelial cells undergoing EndMT can further be induced towards a contractile smooth muscle phenotype, expressing α SMA and calponin; thus, another potential role for EndMT in the placenta could be in the regulation of vessel contractility and placental blood flow. However, further studies to assess the role of EndMT in the placenta are required.

In the present study, we demonstrated that TGF- β 2 and IL-1 β -induced EndMT in HUVECs as exemplified by changes in cellular morphology, a reduction in endothelial cell markers and an increase in mesenchymal markers. This was accompanied by increased expression of *TGFB2* and *TGFB1* (ALK5), as well as the EndMT transcription factors, *SNAI1* and *SNAI2*. This is consistent with other *in vitro* EndMT models (Ma et al., 2021; Maleszewska et al., 2013; Monteiro et al., 2021; Evrard et al., 2016), suggesting that EndMT in fetoplacental

vasculature is probably mediated through the canonical EndMT signalling pathway; however, further work to explore the EndMT signalling mechanisms is required.

In GDM HUVECs, the induction of *TGFB1*, *IL1B* and *IL1R* expression was diminished compared to non-GDM HUVECs, which is consistent with other studies reporting dysregulation of TGF- β and IL-1 β signalling in the GDM placenta (Grissa et al., 2010; Vitoratos et al., 2008; Yener et al., 2007; Zgutka et al., 2024). However, there were no differences in the expression of mesenchymal markers,

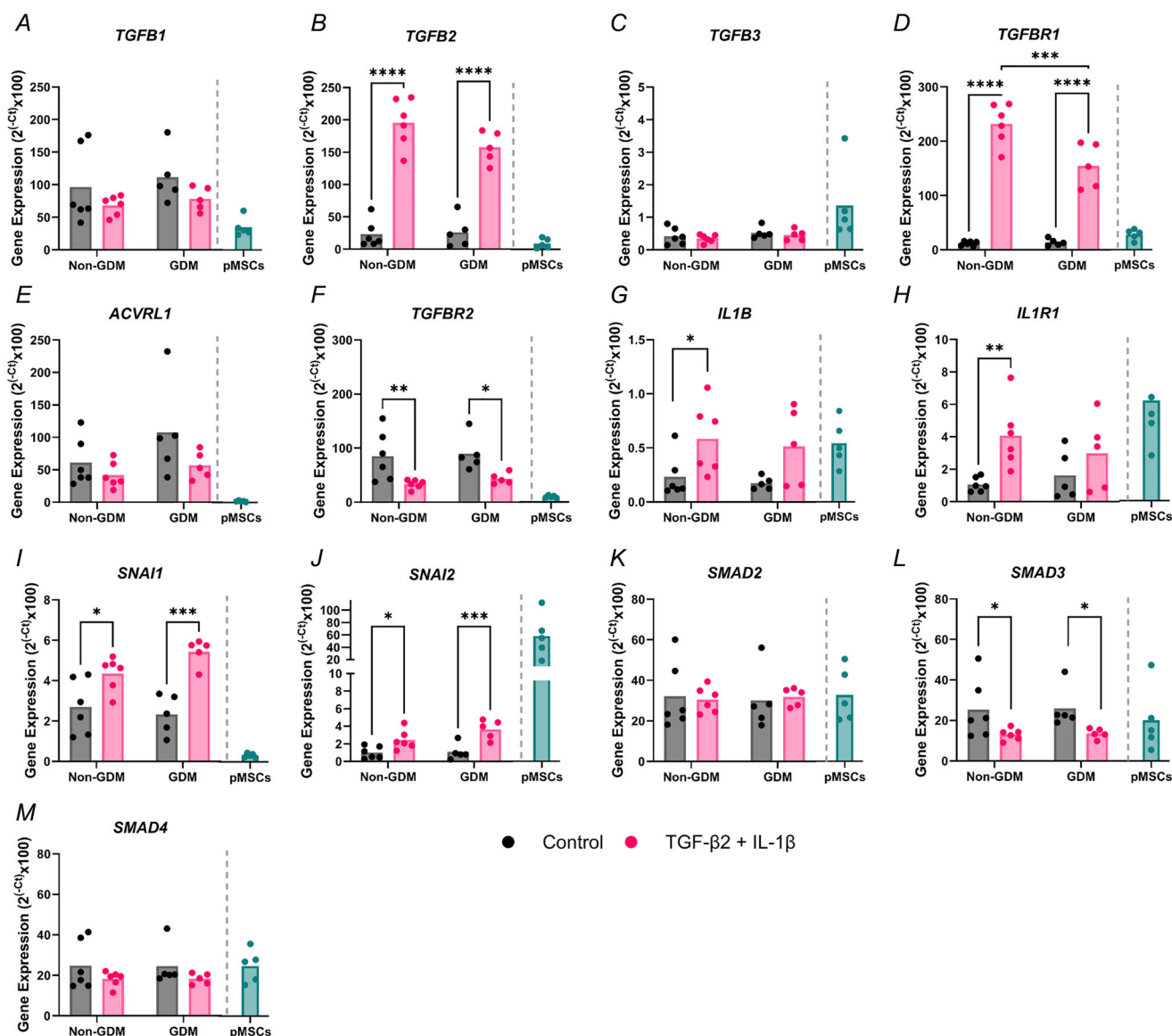
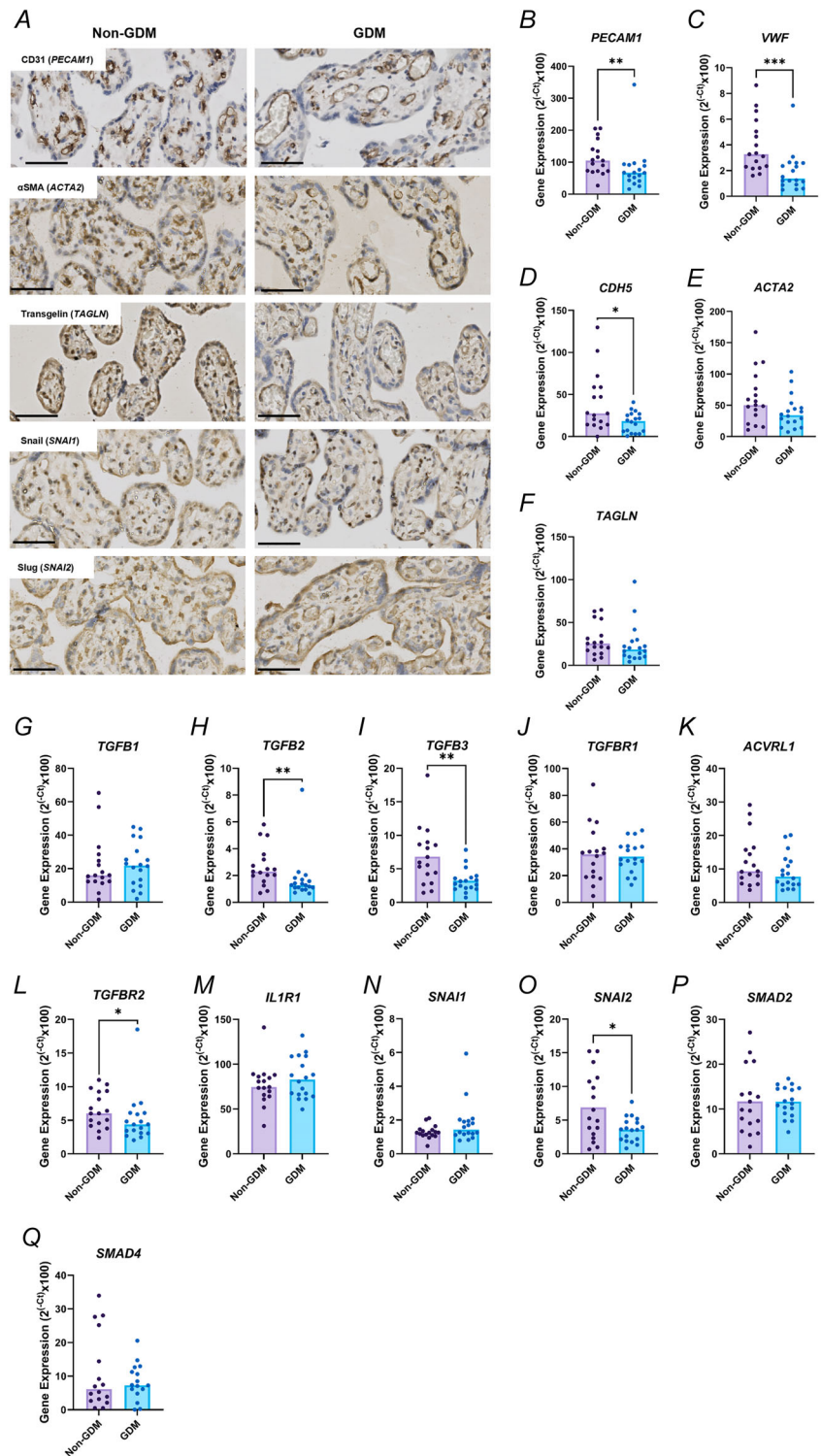


Figure 4. EndMT induction in GDM HUVECs occurs in a similar manner to non-GDM HUVECs

A-M, HUVECs isolated from non-GDM ($n = 6$) and GDM pregnancies ($n = 5$) were cultured in either control medium (EGM-2 only) or treated with EGM-2 containing TGF- β 2 (10 ng mL⁻¹) and IL-1 β (10 ng mL⁻¹) for 6 days. As a mesenchymal cell positive control primary pMSCs were used. Expression of EndMT regulators, transcription factors and signalling molecules were measured via RT-qPCR. Data are presented as the mean. Statistical analysis was performed using two-way ANOVA with a Fisher's *post hoc* test (data that were not normally distributed were log-transformed; * $P < 0.05$, ** $P < 0.01$, *** $P < 0.001$, **** $P < 0.0001$).



EndMT transcription factors or the majority of endothelial markers following EndMT induction.

Although this may suggest that the vascular changes that occur in the GDM placenta are not attributed to EndMT, another possible explanation may be that our study was not powered to assess whether there were

differences in EndMT in GDM placenta that could be linked to adverse outcomes in GDM, such as birthweight. GDM is well documented to result in complications of fetal growth, where babies are born small or large for gestational age (Drever et al., 2023). Boss et al. (2023) demonstrated changes in placental EndMT in fetal growth

Table 4. Maternal and fetal demographic information for placental lysates used.

	Non-GDM (<i>n</i> = 17)	GDM (<i>n</i> = 18)	<i>P</i> value
Maternal age (years) ¹	29.5 ± 5.32	32.4 ± 4.16	0.0791
Booking BMI (kg m⁻²) ¹	29.3 ± 8.89	30.5 ± 6.03 ^a	0.653
Ethnicity	White = 12; Black = 1, Asian = 4	White = 8; Asian = 7; other = 3	0.118
Gestational age (days) ¹	274.5 ± 6.96	270.1 ± 5.52 ^b	0.0507
Parity	P0 = 5 P1 = 6 P2 = 4 P3 = 2	P0 = 3 P1 = 7 P2 = 3 P3 = 2 P≥4 = 3	0.534
Mode of delivery	SVD = 6; ELCS = 10, Unknown = 1	SVD = 3; VD-ind = 2; ELCS = 8; EMCS = 4; unknown = 1	0.109
Placental weight (g) ¹	608.6 ± 133.0 ^b	665.9 ± 257.2	0.429
Birthweight (g) ¹	3810 ± 494.1	3732 ± 629.5	0.685
Birthweight centile³	89.9 (46.65, 96.15)	82.40 (42.48, 97.50) ^b	0.872
Birthweight class²	AGA = 8; LGA = 9	AGA = 10; LGA = 8	0.739
Fetal sex²	Male = 9; female = 8	Male = 9; female = 8; unknown = 1	1.00
GDM medication²	NA	Metformin = 1; diet = 1, not available = 16 ^c	NA

Data are presented as the ¹mean ± standard deviation, ²absolute numbers and ³median (25% percentile, 75% percentile). Statistical analysis was performed using an unpaired *t* test (maternal age, booking BMI, gestational age, placental weight, birthweight; normally distributed continuous data) or Mann–Whitney *U* test (birthweight centile; not normally distributed continuous data) or a Fisher's exact test (ethnicity, parity, mode of delivery, birthweight class, fetal sex; categorical data). Abbreviations: LGA, large for gestational age; AGA, appropriately grown for gestational age; BMI, body mass index; SVD, spontaneous vaginal delivery; VD-ind, induced vaginal delivery; ELCS, elective caesarean section; EMCS, emergency Caesarean section; NA, not applicable. ^a*n* = 17, ^b*n* = 16, ^cnot available (either no medication is prescribed, or no medication was identified in the medical records and available demographics).

restriction (FGR) and Aplin et al. (2015) postulate that EndMT may explain the vascular regression in FGR placenta. This is particularly important to note in the context of our current study given that our HUVECs and placental samples included those from pregnancies with LGA, as well as appropriately grown for gestational age infants. Although we did not assess it in this cohort, the level of maternal glucose control in GDM can affect pregnancy outcomes, including fetal growth (Law et al., 2019; Metzger et al., 2008) and rates of congenital heart disease (Helle et al., 2018); furthermore, hyperglycaemia has been shown to induce EndMT (Fu et al., 2024; Hulshoff et al., 2023; Li et al., 2023; Meng et al., 2023; Tsai et al., 2019, 2021), albeit at supraphysiological levels. It would therefore be interesting to assess EndMT in the context of fetal growth and maternal glucose control in future studies.

Another potential explanation for our findings is that a GDM environment has less of an impact on EndMT in placental macrovasculature than in placental microvasculature, given that glucose levels have been shown to be lower in umbilical cord vein than in placenta or maternal circulation (Holme et al., 2015). Moreover, umbilical vessels are known to differ in their structure

from placental blood vessels (Lang et al., 2008) and *in vitro* HUVECs have altered morphology and responses to endothelial growth factors compared to placental microvascular endothelial cells (Lang et al., 1993), and there also may be differences in venous and arterial endothelial cells from the umbilical cord (Vega-Tapia et al., 2021). Indeed, our observation that the reduction in endothelial cell marker expression (*PECAM1*, *VWF* and *CDH5*) in GDM placental villous tissue was accompanied by a reduction in some EndMT regulators, including *SNAI2*, *TGFB2*, *TGFB3* and *TGFBR2*, supports this hypothesis. However, we saw no changes in mesenchymal markers in the GDM placenta or in other EndMT regulators, which may suggest that these genes have other roles in the placenta. For example, *SNAI2* is also known to regulate vascular remodelling, smooth muscle differentiation, proliferation and migration, as well as endothelial cell functions during angiogenesis (Zhou et al., 2019), suggesting that altered *SNAI2* in the GDM placenta may be linked to other alterations in vascular development. Similarly, *TGF-β*, *IL-1* and *CDH5* (VE-cadherin) are known to play other roles in angiogenesis, vasculogenesis and endothelial barrier function (Babawale et al., 2000; Fahey & Doyle, 2019; Goumans et al., 2009; Leach et al., 2002, 2004); thus,

the lower levels of molecules in these pathways in GDM may be linked to alterations in these processes. It would be of interest to expose placental villous tissue to the EndMT induction protocol to assess changes in *SNAI2*, *CDH5* and other markers. However, studies suggest that vessel integrity is reduced during culture in placental explants (Aplin et al., 2015), which potentially limits the use of explants for studying EndMT, and so studies using isolated placental microvascular endothelial cells may be required to address this.

Overall, the present study is the first to investigate whether a diabetic environment *in utero* has the potential to influence EndMT in the fetoplacental macro- and microvasculature. We show that EndMT markers are present in the human placenta at term, indicating a capacity for EndMT in the placenta. Treatment with TGF- β 2 and IL-1 β induced morphological and molecular changes consistent with EndMT in both non-GDM and GDM macrovasculature. Although we observed that GDM may impact the regulatory mechanisms controlling EndMT in the macrovasculature, we observed no alterations in the level of EndMT induction. In the GDM fetoplacental microvasculature, reduced gene expression of endothelial markers is consistent with altered EndMT; however, there were limited changes in mesenchymal markers and other EndMT regulators and further studies are required to explore this. Our data suggests that, in GDM, although there may be some changes in EndMT regulatory molecules in the fetoplacental vasculature, alterations in EndMT probably do not fully explain the fetoplacental vascular dysfunction and associated complications in the fetus and offspring in pregnancies complicated by GDM.

References

- Aguilera, J., Semmler, J., Anzoategui, S., Zhang, H., Nicolaides, K. H., & Charakida, M. (2021). Cardiac function in gestational diabetes mellitus: A longitudinal study from fetal life to infancy. *British Journal of Obstetrics and Gynaecology*, **128**(2), 272–279.
- Akarsu, S., Bagirzade, M., Omeroglu, S., & Buke, B. (2017). Placental vascularization and apoptosis in type-1 and gestational DM. *Journal of Maternal-Fetal and Neonatal Medicine*, **30**(9), 1045–1050.
- Al-Biltagi, M., El razaky, O., & El Amrousy, D. (2021). Cardiac changes in infants of diabetic mothers. *World Journal of Diabetes*, **12**(8), 1233–1247.
- Anbara, T., Sharifi, M., & Aboutaleb, N. (2019). Endothelial to mesenchymal transition in the cardiogenesis and cardiovascular diseases. *Current Cardiology Reviews*, **16**, 306–314.
- Aplin, J., Swietlik, S., Charnock, J., Khalid, M., Westwood, M., & Johnstone, E. (2015). Vascular regression in the fetoplacental vascular bed, and its possible implications for fetal growth restriction. *Placenta*, **36**(4), 472.
- Babawale, M. O., Lovat, S., Mayhew, T. M., Lammiman, M. J., James, D. K., & Leach, L. (2000). Effects of gestational diabetes on junctional adhesion molecules in human term placental vasculature. *Diabetologia*, **43**(9), 1185–1196.
- Balsells, M., García-Patterson, A., Gich, I., & Corcoy, R. (2012). Major congenital malformations in women with gestational diabetes mellitus: A systematic review and meta-analysis. *Diabetes Metabolism Research and Reviews*, **28**(3), 252–257.
- Bankhead, P., Loughrey, M. B., Fernández, J. A., Dombrowski, Y., McArt, D. G., Dunne, P. D., McQuaid, S., Gray, R. T., Murray, L. J., Coleman, H. G., James, J. A., Salto-Tellez, M., & Hamilton, P. W. (2017). QuPath: Open source software for digital pathology image analysis. *Scientific Reports*, **7**(1), 16878.
- Bellehumeur, C., Blanchet, J., Fontaine, J. Y., Bourcier, N., & Akoum, A. (2009). Interleukin 1 regulates its own receptors in human endometrial cells via distinct mechanisms. *Human Reproduction*, **24**(9), 2193–2204.
- Bhattacharjee, D., Mondal, S. K., Garain, P., Mandal, P., Ray, R. N., & Dey, G. (2017). Histopathological study with immunohistochemical expression of vascular endothelial growth factor in placentas of hyperglycemic and diabetic women. *Journal of Laboratory Physicians*, **9**, 227–233.
- Bischoff, J. (2019). Endothelial-to-mesenchymal transition. *Circulation Research*, **124**(8), 1163–1165.
- Böhrnsen, F., & Schliephake, H. (2016). Supportive angiogenic and osteogenic differentiation of mesenchymal stromal cells and endothelial cells in monolayer and co-cultures. *International Journal of Oral Science*, **8**(4), 223–230.
- Boss, A. L., Chamley, L. W., Brooks, A. E. S., & James, J. L. (2023). Human placental vascular and perivascular cell heterogeneity differs between first trimester and term, and in pregnancies affected by foetal growth restriction. *Molecular Human Reproduction*, **29**(12), gaad041.
- Bronson, R., Lyu, J., & Xiong, J. (2023). Transcriptome analysis reveals molecular signature and cell-type difference of homo sapiens endothelial-to-mesenchymal transition. *G3: Genes, Genomes, Genetics*, **13**(12), jkad243.
- Byford, A., Baird-Rayner, C., & Forbes, K. (2021). Don't sugar coat it: The effects of gestational diabetes on the placental vasculature. *Biochemical (London)*, **43**(2), 34–39.
- Calderon, I. M. P., Damasceno, D. C., Amorin, R. L., Costa, R. A. A., Brasil, M. A. M., & Rudge, M. V. C. (2007). Morphometric study of placental villi and vessels in women with mild hyperglycemia or gestational or overt diabetes. *Diabetes Research and Clinical Practice*, **78**(1), 65–71.
- Chen, A., Tan, B., Du, R., Chong, Y. S., Zhang, C., Koh, A. S., & Li, L. J. (2024). Gestational diabetes mellitus and development of intergenerational overall and subtypes of cardiovascular diseases: A systematic review and meta-analysis. *Cardiovascular Diabetology*, **23**(1), 1–15.
- Chen, L., He, J., Zhang, Y., Li, Y., Zhang, T., Wang, R., Bai, L., Zhao, S., Liu, E., & Wang, W. (2023). Regulation of endothelial-to-mesenchymal transition by histone deacetylase 3 posttranslational modifications in neointimal hyperplasia. *Annals of Translational Medicine*, **11**(5), 207–207.

- Cvitic, S., Novakovic, B., Gordon, L., Ulz, C. M., Mühlberger, M., Diaz-Perez, F. I., Joo, J. E., Svendova, V., Schimek, M. G., Trajanoski, S., Saffery, R., Desoye, G., & Hiden, U. (2018). Human fetoplacental arterial and venous endothelial cells are differentially programmed by gestational diabetes mellitus, resulting in cell-specific barrier function changes. *Diabetologia*, **61**(11), 2398–2411.
- Daskalakis, G., Marinopoulos, S., Krielesi, V., Papapanagiotou, A., Papantoniou, N., Mesogitis, S., & Antsaklis, A. (2008). Placental pathology in women with gestational diabetes. *Acta Obstetrica Et Gynecologica Scandinavica*, **87**(4), 403–407.
- Demir, R., Seval, Y., & Huppertz, B. (2007). Vasculogenesis and angiogenesis in the early human placenta. *Acta Histochemica*, **109**(4), 257–265.
- Depla, A. L., De Wit, L., Steenhuis, T. J., Sliker, M. G., Voormolen, D. N., Scheffer, P. G., De Heus, R., Van Rijn, B. B., & Bekker, M. N. (2021). Effect of maternal diabetes on fetal heart function on echocardiography: Systematic review and meta-analysis. *Ultrasound in Obstetrics & Gynecology: The Official Journal of the International Society of Ultrasound in Obstetrics and Gynecology*, **57**(4), 539–550.
- Diniz, M. S., Hiden, U., Falcão-Pires, I., Oliveira, P. J., Sobrevia, L., & Pereira, S. P. (2023). Fetoplacental endothelial dysfunction in gestational diabetes mellitus and maternal obesity: A potential threat for programming cardiovascular disease. *Biochimica et Biophysica Acta - Molecular Basis of Disease*, **1869**(8), 166834.
- Drever, H. J., Davidson, S. J., Callaway, L. K., Sekar, R., & De Jersey, S. J. (2023). Factors associated with higher risk of small-for-gestational-age infants in women treated for gestational diabetes. *Australian and New Zealand Journal of Obstetrics and Gynaecology*, **63**(5), 714–720.
- Ehlers, E., Talton, O. O., Schust, D. J., & Schulz, L. C. (2021). Placental structural abnormalities in gestational diabetes and when they develop: A scoping review. *Placenta*, **116**, 58–66.
- Evrard, S. M., Lecce, L., Michelis, K. C., Nomura-Kitabayashi, A., Pandey, G., Purushothaman, K. R., d'Escamard, V., Li, J. R., Hadri, L., Fujitani, K., Moreno, P. R., Benard, L., Rimmele, P., Cohain, A., Mecham, B., Randolph, G. J., Nabel, E. G., Hajjar, R., Fuster, V., ... Kovacic, J. C. (2016). Endothelial to mesenchymal transition is common in atherosclerotic lesions and is associated with plaque instability. *Nature Communications*, **7**(1), 11853.
- Fahey, E., & Doyle, S. L. (2019). IL-1 family cytokine regulation of vascular permeability and angiogenesis. *Frontiers in Immunology*, **10**, 1426.
- Ferreira, F. U., Souza, L. E. B., Thomé, C. H., Pinto, M. T., Origassa, C., Salustiano, S., Faça, V. M., Câmara, N. O., Kashima, S., & Covas, D. T. (2019). Endothelial cells tissue-specific origins affects their responsiveness to TGF- β 2 during endothelial-to-mesenchymal transition. *International Journal of Molecular Sciences*, **20**(3), 458.
- Forbes, K., Westwood, M., Baker, P. N., & Aplin, J. D. (2008). Insulin-like growth factor I and II regulate the life cycle of trophoblast in the developing human placenta. *American Journal of Physiology-Cell Physiology*, **294**(6), C1313–C1322.
- Fu, T. L., Li, G. R., Li, D. H., He, R. Y., Liu, B. H., Xiong, R., Xu, C. Z., Lu, Z. L., Song, C. K., Qiu, H. L., Wang, W. J., Zou, S. S., Yi, K., Li, N., & Geng, Q. (2024). Mangiferin alleviates diabetic pulmonary fibrosis in mice via inhibiting endothelial-mesenchymal transition through AMPK/FoxO3/SIRT3 axis. *Acta Pharmacologica Sinica*, **45**(5), 1002–1018.
- Gordon, B., González-Fernández, V., & Dos-Subirà, L. (2022). Myocardial fibrosis in congenital heart disease. *Frontiers in Pediatrics*, **80**(6), 1300–1307.
- Goumans, M. J., Liu, Z., & Ten Dijke, P. (2009). TGF- β signaling in vascular biology and dysfunction. *Cell Research*, **19**(1), 116–127.
- Grissa, O., Yessoufou, A., Mrisak, I., Hichami, A., Amoussou-Guenou, D., Grissa, A., Djrolo, F., Moutairou, K., Miled, A., Khairi, H., Zaouali, M., Bougmiza, I., Zbidi, A., Tabka, Z., & Khan, N. A. (2010). Growth factor concentrations and their placental mRNA expression are modulated in gestational diabetes mellitus: Possible interactions with macrosomia. *BioMed Central Pregnancy Childbirth*, **10**(1), 7.
- Helle, E. I. T., Biegley, P., Knowles, J. W., Leader, J. B., Pendergrass, S., Yang, W., Reaven, G. R., Shaw, G. M., Ritchie, M., & Priest, J. R. (2018). First trimester plasma glucose values in women without diabetes are associated with risk for congenital heart disease in offspring. *Journal of Pediatrics*, **195**, 275–278.
- Holme, A. M., Roland, M. C. P., Lorentzen, B., Michelsen, T. M., & Henriksen, T. (2015). Placental glucose transfer: A human in vivo study. *PLoS ONE*, **10**(2), e0117084.
- Hulshoff, M. S., Schellinger, I. N., Xu, X., Fledderus, J., Rath, S. K., Wong, F. C., Maamari, S., Haunschild, J., Krenning, G., Raaz, U., & Zeisberg, E. M. (2023). miR-132-3p and KLF7 as novel regulators of aortic stiffening-associated EndMT in type 2 diabetes mellitus. *Diabetology & Metabolic Syndrome*, **15**(1), 11.
- James, J. L., Boss, A. L., Sun, C., Allerkamp, H. H., & Clark, A. R. (2022). From stem cells to spiral arteries: A journey through early placental development. *Placenta*, **125**, 68–77.
- Jirkovská, M., Kučera, T., Kaláb, J., Jadrníček, M., Niedobová, V., Janáček, J., Kubínová, L., Moravcová, M., Žizka, Z., & Krejčí, V. (2012). The branching pattern of villous capillaries and structural changes of placental terminal villi in type 1 diabetes mellitus. *Placenta*, **33**(5), 343–351.
- Junaid, T. O., Brownbill, P., Chalmers, N., Johnstone, E. D., & Aplin, J. D. (2014). Fetoplacental vascular alterations associated with fetal growth restriction. *Placenta*, **35**(10), 808–815.
- Kennedy, M. G. (2022). Circulating miRNAs as key regulators of placental vascular dysfunction and altered fetal growth in pregnancies complicated by diabetes (*thesis*). University of Leeds.
- Kovacic, J. C., Dimmeler, S., Harvey, R. P., Finkel, T., Aikawa, E., Krenning, G., & Baker, A. H. (2019). Endothelial to mesenchymal transition in cardiovascular disease: JACC state-of-the-art review. *Journal of the American College of Cardiology*, **73**(2), 190–209.

- Kramer, C. K., Campbell, S., & Retnakaran, R. (2019). Gestational diabetes and the risk of cardiovascular disease in women: A systematic review and meta-analysis. *Diabetologia*, **62**(6), 905–914.
- Lang, I., Hartmann, M., Blaschitz, A., Dohr, G., Skofitsch, G., & Desoye, G. (1993). Immunohistochemical evidence for the heterogeneity of maternal and fetal vascular endothelial cells in human full-term placenta. *Cell and Tissue Research*, **274**(2), 211–218.
- Lang, I., Schweizer, A., Hiden, U., Ghaffari-Tabrizi, N., Hagendorfer, G., Bilban, M., Pabst, M. A., Korgun, E. T., Dohr, G., & Desoye, G. (2008). Human fetal placental endothelial cells have a mature arterial and a juvenile venous phenotype with adipogenic and osteogenic differentiation potential. *Differentiation*, **76**(10), 1031–1043.
- Law, G. R., Alnaji, A., Alrefaii, L., Endersby, D., Cartland, S. J., Gilbey, S. G., Jennings, P. E., Murphy, H. R., & Scott, E. M. (2019). Suboptimal nocturnal glucose control is associated with large for gestational age in treated gestational diabetes mellitus. *Diabetes Care*, **42**(5), 810–815.
- Leach, L., Babawale, M. O., Anderson, M., & Lammiman, M. (2002). Vasculogenesis, angiogenesis and the molecular organisation of endothelial junctions in the early human placenta. *Journal of Vascular Research*, **39**(3), 246–259.
- Leach, L., Gray, C., Staton, S., Babawale, M. O., Gruchy, A., Foster, C., Mayhew, T. M., & James, D. K. (2004). Vascular endothelial cadherin and β -catenin in human fetoplacental vessels of pregnancies complicated by type 1 diabetes: Associations with angiogenesis and perturbed barrier function. *Diabetologia*, **47**(4), 695–709.
- Li, Y., Zhao, Y., Song, L., Xiong, L., Li, W., Wu, W., & Miao, L. (2023). High glucose levels contribute to vascular fibrosis via the activation of the endothelial-to-mesenchymal transition in periodontitis. *Journal of Periodontal Research*, **58**(2), 225–236.
- Liu, Y., Yue, L., & Chang, L. (2024). Maternal gestational diabetes mellitus and congenital heart disease in offspring: A meta-analysis. *Hormone and Metabolic Research*, **56**(08), 574–584.
- Ma, J., van der Zon, G., Gonçalves, M., van Dinther, M., Thorikay, M., Sanchez-Duffhues, G., & ten Dijke, P. (2021). TGF- β -induced endothelial to mesenchymal transition is determined by a balance between SNAIL and ID factors. *Frontiers in Cell and Developmental Biology*, **9**, 616610.
- Mahadevan, A., Tipler, A., & Jones, H. (2023). Shared developmental pathways of the placenta and fetal heart. *Placenta*, **141**, 35–42.
- Maleszewska, M., Moonen, J., Huijckman, N., van de Sluis, B., Krenning, G., & Harmsen, M. C. (2013). IL-1 β and TGF β 2 synergistically induce endothelial to mesenchymal transition in an nf κ b-dependent manner. *Immunobiology*, **218**(4), 443–454.
- Markwald, R. R., Fitzharris, T. P., & Manasek, F. J. (1977). Structural development of endocardial cushions. *American Journal of Anatomy*, **148**(1), 85–119.
- Markwald, R. R., Fitzharris, T. P., & Smithy, W. N. A. (1975). Structural analysis of endocardial cytodifferentiation. *Developmental Biology*, **42**(1), 160–180.
- Meng, Z., Shen, W., Yu, L., Tong, F., He, H., Hu, Y., Wu, W., & Liu, J. (2023). Bach1 modulates AKT3 transcription to participate in hyperglycaemia-mediated EndMT in vascular endothelial cells. *Clinical and Experimental Pharmacology & Physiology*, **50**(6), 443–452.
- Metzger, B. E., Lowe, L. P., Dyer, A. R., Trimble, E. R., Chaovarindr, U., Coustan, D. R., Hadden, D. R., McCance, D. R., Hod, M., McIntyre, H. D., Oats, J. J., Persson, B., Rogers, M. S., & Sacks, D. A. (2008). Hyperglycemia and adverse pregnancy outcomes. *New England Journal of Medicine*, **358**, 1991–2002.
- Monteiro, J. P., Rodor, J., Caudrillier, A., Scanlon, J. P., Spiroski, A. M., Dudnakova, T., Pflüger-Müller, B., Shmakova, A., von Kriegsheim, A., Deng, L., Taylor, R. S., Wilson-Kanamori, J. R., Chen, S. H., Stewart, K., Thomson, A., Mitić, T., McClure, J. D., Iynikell, J., Hadoke, P. W. F., ... Baker, A. H. (2021). MIR503HG loss promotes endothelial-to-mesenchymal transition in vascular disease. *Circulation Research*, **128**(8), 1173–1190.
- NICE. (2015). New thresholds for diagnosis of diabetes in pregnancy. Available at: <https://www.nice.org.uk/news/article/new-thresholds-for-diagnosis-of-diabetes-in-pregnancy> [Accessed May 13, 2020].
- Pelekanos, R. A., Sardesai, V. S., Futrega, K., Lott, W. B., Kuhn, M., & Doran, M. R. (2016). Isolation and expansion of mesenchymal stem/stromal cells derived from human placenta tissue. *Journal of Visualized Experiments*, **2016**, 1–3.
- Pérez, L., Muñoz-Durango, N., Riedel, C. A., Echeverría, C., Kalergis, A. M., Cabello-Verrugio, C., & Simon, F. (2017). Endothelial-to-mesenchymal transition: Cytokine-mediated pathways that determine endothelial fibrosis under inflammatory conditions. *Cytokine & Growth Factor Reviews*, **33**, 41–54.
- Piera-Velazquez, S., & Jimenez, S. A. (2019). Endothelial to mesenchymal transition: Role in physiology and in the pathogenesis of human diseases. *Physiological Reviews*, **99**(2), 1281–1324.
- Pinto, M. T., Covas, D. T., Kashima, S., & Rodrigues, C. O. (2016). Endothelial mesenchymal transition: Comparative analysis of different induction methods. *Biological Procedures Online*, **18**(1), 1–8.
- Singh, A., Bhatt, K. S., Nguyen, H. C., Frisbee, J. C., & Singh, K. K. (2024). Endothelial-to-mesenchymal transition in cardiovascular pathophysiology. *International Journal of Molecular Sciences*, **25**(11), 6180.
- Sobrevia, L., Abarzúa, F., Nien, J. K., Salomón, C., Westermeier, F., Puebla, C., Cifuentes, F., Guzmán-Gutiérrez, E., Leiva, A., & Casanello, P. (2011). Review: Differential placental macrovascular and micro-vascular endothelial dysfunction in gestational diabetes. *Placenta*, **32**(Suppl 2), S159–S164.
- Stoz, F., Schuhmann, R. A., & Schultz, R. (1988). Morphohistometric investigations of placentas of diabetic patients in correlation to the metabolic adjustment of the disease. *Journal of Perinatal Medicine*, **16**(3), 211–216.

- Terzuoli, E., Nannelli, G., Giachetti, A., Morbidelli, L., Ziche, M., & Donnini, S. (2020). Targeting endothelial-to-mesenchymal transition: The protective role of hydroxytyrosol sulfate metabolite. *European Journal of Nutrition*, **59**(2), 517–527.
- Tian, J., Zhang, M., Suo, M., Liu, D., Wang, X., Liu, M., Pan, J., Jin, T., & An, F. (2021). Dapagliflozin alleviates cardiac fibrosis through suppressing EndMT and fibroblast activation via $\text{ampk}\alpha/\text{TGF-}\beta/\text{smad}$ signalling in type 2 diabetic rats. *Journal of Cellular and Molecular Medicine*, **25**(16), 7642–7659.
- Troncoso, F., Acurio, J., Herlitz, K., Aguayo, C., Bertoglia, P., Guzman-Gutierrez, E., Loyola, M., Gonzalez, M., Rezgaoui, M., Desoye, G., & Escudero, C. (2017). Gestational diabetes mellitus is associated with increased pro-migratory activation of vascular endothelial growth factor receptor 2 and reduced expression of vascular endothelial growth factor receptor 1. *PLoS ONE*, **12**(8), e0182509.
- Tsai, T. H., Lee, C. H., Cheng, C. I., Fang, Y. N., Chung, S. Y., Chen, S. M., Lin, C. J., Wu, C. J., Hang, C. L., & Chen, W. Y. (2019). Liraglutide inhibits endothelial-to-mesenchymal transition and attenuates neointima formation after end-ovascular injury in streptozotocin-induced diabetic mice. *Cells*, **8**(6), 589.
- Vega-Tapia, F., Peñaloza, E., & Krause, B. J. (2021). Specific arterio-venous transcriptomic and ncRNA-RNA interactions in human umbilical endothelial cells: A meta-analysis. *Iscience*, **24**(6), 102675.
- Venkataraman, H., Ram, U., Craik, S., Arungunasekaran, A., Seshadri, S., & Saravanan, P. (2016). Increased fetal adiposity prior to diagnosis of gestational diabetes in South Asians: More evidence for the 'thin-fat' baby. *Diabetologia*, **60**(3), 399.
- Villota, S. D., Toledo-Rodriguez, M., & Leach, L. (2021). Compromised barrier integrity of human feto-placental vessels from gestational diabetic pregnancies is related to downregulation of occludin expression. *Diabetologia*, **64**(1), 195–210.
- Vitoratos, N., Professor, A., Vitoratos, N., Valsamakis, G., Mastorakos, G., Boutsiadis, A., Salakos, N., Kouskouni, E., & Creatsas, G. (2008). *Pre-and early post-partum adiponectin and Interleukin-1beta levels in women with and without gestational diabetes*.
- Wang, C., Li, Y., Yang, M., Zou, Y., Liu, H., Liang, Z., Yin, Y., Niu, G., Yan, Z., & Zhang, B. (2018). Efficient differentiation of bone marrow mesenchymal stem cells into endothelial cells in vitro. *European Journal of Vascular and End-ovascular Surgery*, **55**(2), 257–265.
- Wang, E., Wang, H., & Chakrabarti, S. (2023). Endothelial-to-mesenchymal transition: An under-appreciated mediator of diabetic complications. *Frontiers in Endocrinology (Lausanne)*, **14**, 1050540.
- Wang, H., Li, N., Chivese, T., Werfalli, M., Sun, H., Yuen, L., Hoegfeldt, C. A., Elise Powe, C., Immanuel, J., Karuranga, S., Divakar, H., Levitt, N. A., Li, C., Simmons, D., & Yang, X. (2022). IDF diabetes atlas: Estimation of global and regional gestational diabetes mellitus prevalence for 2021 by international association of diabetes in pregnancy study group's criteria. *Diabetes Research and Clinical Practice*, **183**, 109050.
- Wang, J. J., Wang, X., Li, Q., Huang, H., Zheng, Q. L., Yao, Q., & Zhang, J. (2023). Feto-placental endothelial dysfunction in gestational diabetes mellitus under dietary or insulin therapy. *BioMed Central Endocrine Disorders*, **23**(1), 48.
- Wang, Y., & Zhao, S. (2010). *Vascular Biology of the Placenta*.
- Xu, X., Tan, X., Tampe, B., Sanchez, E., Zeisberg, M., & Zeisberg, E. M. (2015). Snail is a direct target of hypoxia-inducible factor 1 α (HIF1 α) in hypoxia-induced endothelial to mesenchymal transition of human coronary endothelial cells. *Journal of Biological Chemistry*, **290**(27), 16653–16664.
- Yener, S., Demir, T., Akinci, B., Bayraktar, F., Kebapcilar, L., Ozcan, M. A., Biberoglu, S., & Yesil, S. (2007). Transforming growth factor-beta 1 levels in women with prior history of gestational diabetes mellitus. *Diabetes Research and Clinical Practice*, **76**(2), 193–198.
- Yoshimatsu, Y., Wakabayashi, I., Kimuro, S., Takahashi, N., Takahashi, K., Kobayashi, M., Maishi, N., Podyma-Inoue, K. A., Hida, K., Miyazono, K., & Watabe, T. (2020). TNF- α enhances TGF- β -induced endothelial-to-mesenchymal transition via TGF- β signal augmentation. *Cancer Science*, **111**(7), 2385–2399.
- Yu, H., Mrowietz, U., & Seifert, O. (2009). Downregulation of SMAD2, 4 and 6 mRNA and $\text{tgf}\beta$ receptor I mRNA in lesional and non-lesional psoriatic skin. *Acta Dermato-Venereologica*, **89**(4), 351–356.
- Zgutka, K., Tkacz, M., Tomasiak, P., Piotrowska, K., Ustianowski, P., Pawlik, A., & Tarnowski, M. (2024). Gestational diabetes mellitus-induced inflammation in the placenta via IL-1 β and toll-like receptor pathways. *International Journal of Molecular Sciences*, **25**(21), 11409.
- Zhou, J., Ni, X., Huang, X., Yao, J., He, Q., Wang, K., & Duan, T. (2016). Potential role of hyperglycemia in fetoplacental endothelial dysfunction in gestational diabetes mellitus. *Cellular Physiology and Biochemistry*, **39**(4), 1317–1328.
- Zhou, W., Gross, K. M., & Kuperwasser, C. (2019). Molecular regulation of Snai2 in development and disease. *Journal of Cell Science*, **132**(23), jcs235127.
- Zhu, X., Wang, Y., Soaita, I., Lee, H. W., Bae, H., Boutagy, N., Bostwick, A., Zhang, R. M., Bowman, C., Xu, Y., Trefely, S., Chen, Y., Qin, L., Sessa, W., Tellides, G., Jang, C., Snyder, N. W., Yu, L., Arany, Z., & Simons, M. (2023). Acetate controls endothelial-to-mesenchymal transition. *Cell Metabolism*, **35**(7), 1163–1178.e10.

Additional information

Data availability statement

All data underlying the results are available as part of the article and no additional source data are required.

Competing interests

The authors declare that they have no competing interests.

Author contributions

K.F conceptualised the study, with input from A.R.B and G.F. K.F and E.M.S secured funding. K.F, A.R.B, E.M.S and B.H supervised all aspects of the study. Z.S and S.S contributed to experiments and data acquisition. A.R.B and G.F performed experiments and analysed and interpreted all data sets. M.B, S.L.E and L.C.M contributed to the isolation of HUVECs. A.R.B, G.F and K.F wrote the manuscript with input from all authors. All authors approved the final version of the manuscript submitted for publication, and agree to be accountable for all aspects of the work in ensuring that questions related to the accuracy or integrity of any part of the work are appropriately investigated and resolved. All persons designated as authors qualify for authorship, and all those who qualify for authorship are listed.

Funding

GF was funded by a University of Leeds Doctoral Scholarship. LCM and SLE were supported in part by the Tommy's (The Pregnancy and Baby Charity) Preterm Birth Centre. LCM was supported by a NIHR Academic Clinical Lectureship. MB is funded by King Saud bin Abdulaziz University for Health Sciences. The work conducted in this study was supported by funding from UK Research and Innovation (UKRI) Medical Research Council (REF:MR/R023166/1; awarded to KF and Ref: MR/Y003659/1; awarded to KF and ES). For the purpose of open access, the authors have applied a CC BY public copyright license

to any Author Accepted Manuscript version arising from this submission.

Acknowledgements

We thank Margeurite Kennedy for contributing to the pMSC isolations. Flow cytometry and microscopy was performed in The Bioimaging Core Facility, Faculty of Biological Sciences, University of Leeds. We thank the participants for the donation of their placentas to the study. We also thank the staff in the delivery units at Leeds General Infirmary and St James University Hospital, Leeds Teaching Hospitals NHS Trust and St Mary's Hospital, Manchester University NHS Foundation Trust.

Keywords

endothelial-to-mesenchymal transition, fetoplacental endothelium, gestational diabetes mellitus, GDM, macrovasculature, microvasculature, placenta, umbilical cord

Supporting information

Additional supporting information can be found online in the Supporting Information section at the end of the HTML view of the article. Supporting information files available:

Peer Review History